biomass

MDPI

Article

Kinetics, Thermodynamics, and the Reaction Mechanism of Common Nigerian Waste Biomass for Pyrolysis-Based Resource Utilisation

Peter Akhator [1,*] and Rita Okpuwhara [2]

[1] Department of Mechanical Engineering, University of Benin, Benin City P.M.B. 1154, Nigeria
[2] Department of Chemical Engineering Technology, University of Johannesburg, Johannesburg P.O. Box 2028, South Africa; 218050287@student.uj.ac.za
* Correspondence: peter.akhator@uniben.edu

Abstract

Pyrolysis presents a promising approach to harness the bioenergy potential of biomass and promote waste valorisation within a circular economy framework. This study offers a detailed analysis of the thermal characteristics, reaction kinetics, and thermodynamic behaviour of two common waste biomasses in Nigeria, sawdust (SD) and sugarcane bagasse (SB), to assess their bioenergy potential using Thermogravimetric Analysis and the Coats-Redfern integral method. Proximate analyses revealed a high volatile matter content (over 82%) in both feedstocks. The pyrolysis parameters indicated a higher comprehensive pyrolysis (3.486×10^{-6}, $\%^3/°C^3$) and pyrolysis stability ($1002.04\%/C^2$) indices for SD, confirming its superior overall thermal reactivity. In contrast, SB demonstrated a superior devolatilisation index ($5.0621 \times 10^{-7}\%/C^3$) and a lower stability index ($869.27\%/C^2$), signifying an intense, concentrated eruption of volatile matter over a narrow temperature window. A multi-stage, segmented approach produced more accurate results than the general single-step model. The diffusion-based D6 model was most suitable for describing the drying and devolatilisation of SD, while the reaction-order R2 model best explained the devolatilisation process of SB. The thermodynamic analysis revealed that formation of the activated complexes for both SD and SB across all stages is strictly non-spontaneous and endothermic, with SD encountering a higher thermal barrier (ΔH = 57.57 kJ/mol) than SB (ΔH = 37.03 kJ/mol) during the process. These findings indicate that SD possesses properties favourable for fast pyrolysis processes aimed at bio-oil production, whereas SB exhibits characteristics that make it a promising feedstock for biochar-orientated pyrolysis. Further studies involving product yield and quality analyses are recommended to validate these potential applications. These findings provide essential information for designing effective, locally adapted bioenergy systems in Sub-Saharan Africa.

Keywords: coats-redfern method; pyrolysis; reaction mechanism; sawdust; sugarcane bagasse; thermogravimetric analysis

Check for updates

Academic Editor: Maurizio Volpe

Received: 5 August 2026
Revised: 28 August 2026
Accepted: 2 September 2026
Published: 7 September 2026

Copyright: © 2026 by the authors. Licensee MDPI, Basel, Switzerland. This article is an open access article distributed under the terms and conditions of the Creative Commons Attribution (CC BY) license.

1. Introduction

Nigeria's growing sugar and wood industries produce substantial quantities of bagasse and sawdust. Nigeria generates approximately 1.8 million tonne of sawdust annually, alongside about 5.2 million tonne of other wood waste [1]. At the same time, limited operational sugar processing mills and restricted local capacity to utilise bagasse have consequently led

to large volumes of bagasse being either discarded or burnt inefficiently, leading to environmental concerns and missed opportunities for energy recovery [2]. These wastes are often poorly managed, leading to environmental issues [2–4]. Typically, sugarcane processing industries in Nigeria utilise sugarcane bagasse for on-site energy generation. However, substantial volumes of bagasse remain underutilised and are therefore dumped into the environment, creating significant waste management and environmental challenges. The sawdust is usually burnt in the open air at industrial sites or disposed of into water bodies by industries located close to rivers, with adverse consequences for humans, animals, and the environment. This emphasises the need for sustainable and innovative methods of waste management. Waste-to-biofuel conversion is a promising technology that aligns with Nigeria's biotechnology initiatives, which aim to achieve a zero-waste economy and develop waste-prevention industries [5].

Thermochemical methods, such as gasification and pyrolysis, provide an eco-friendly approach to biomass valorisation by converting waste into high-value chemicals and biofuels [6–8]. These techniques support a circular bioeconomy and decrease the need for traditional waste disposal [9–11]. To understand these thermal conversions, Thermogravimetric Analysis (TGA) is used to examine degradation stages and reaction kinetics [12,13]. Researchers utilise both model-free and model-fitting approaches to describe biomass pyrolysis kinetics [14–16]. Model-free methods, including Friedman, Flynn-Wall-Ozawa (FWO), Kissinger-Akahira-Sunose (KAS), and Starink, do not assume a specific reaction mechanism, making them flexible across varying heating rates and temperatures [17,18]. However, they require extensive experimental data and computational effort. In contrast, model-fitting methods such as Coats-Redfern [19–21], Distributed Activation Energy Model (DAEM) [22–24], Arrhenius-based models [25,26], Kennedy-Clark [21], and Criado master plot [21,27,28] describe reaction behaviour using predefined kinetic mechanisms.

The Coats-Redfern model-fitting method was employed in this study due to its simplicity, reliability, and effectiveness under non-isothermal conditions typical of biomass pyrolysis [29]. By linearising the Arrhenius equation, the method enables efficient estimation of key kinetic parameters, including activation energy and the pre-exponential factor, using relatively few experimental data points [20,29]. Its practicality and proven applicability make it a widely used approach for evaluating the pyrolysis behaviour of different biomass feedstocks [19,30,31].

Grasping the thermodynamic and kinetic behaviour of biomass is vital for industrial scaling, as these factors dictate energy needs, reaction mechanisms, and product yields [32–34]. Key variables, including reaction order (n), activation energy (Ea), and the pre-exponential factor (A), are essential for designing efficient reactors and operational strategies [15,35,36]. Furthermore, these data enable precise control of temperature and residence time to maximise product quality and accurate energy forecasting to improve overall efficiency [37–39]. Thermodynamic indicators such as Gibbs free energy (ΔG), enthalpy (ΔH), and entropy (ΔS) are vital for analysing heat transfer and energy dynamics during pyrolysis [40–42]. This information is essential for predicting product stability and yields, which assists in optimising the process and designing energy-efficient systems [27,43,44]. Furthermore, thermodynamic assessments help determine the viability of different biomass feedstocks and establish the best processing conditions [45,46]. A holistic understanding of biomass valorisation relies on the interplay between thermodynamic and kinetic data [47,48]. Integrating these factors allows for the creation of predictive models, better reactor performance, and more accurate economic evaluations, all of which are necessary for the commercial success of pyrolysis technologies [49,50]. Ultimately, accurately defining these parameters supports the development of sustainable conversion methods that foster a circular economy and reduce fossil fuel dependency [51–53].

A critical review of the literature reveals that most studies on Nigerian waste biomasses, including sawdust (SD) and sugarcane bagasse (SB), focused mainly on analyses of proximate, ultimate, and calorific values [54]. Several case studies, such as those by Akinrinola, et al. [55], evaluated five local energy crops using proximate, ultimate, and ash-fusion analyses, contrasting them with biomass from the United Kingdom. Similarly, Olivia and Oti Wilberforce [56] characterised ten indigenous biomass types, comparing their elemental and proximate compositions, calorific values, and morphological profiles with those of coal. Other studies include Balogun, et al. [57], who analysed the combustion properties and elemental composition of araba and sorghum husks, and Efetobor, et al. [58], who utilised structural and thermal analyses to assess the potential of elephant grass as a feedstock for bio-oil. Notably, these studies characterised Nigerian biomasses for their bioenergy potentials using elemental properties and energy contents. However, there is a notable dearth of data on kinetic behaviour and the thermodynamic triplet: Gibbs free energy (ΔG), enthalpy (ΔH), and entropy (ΔS), which are essential for rational reactor design, scale-up, and energy efficiency. This information is critical, as biomass properties are highly location-specific, influenced by regional factors such as climate, soil composition, and agricultural practices. Consequently, data derived from other regions, such as South American biomass [59,60] or Asian feedstocks [15,61], may not be applicable to the West African scenario, particularly in Nigeria. Without such localised information, it is difficult to accurately predict reaction spontaneity, thermal equilibrium, energy requirements, residence time, and ultimately the yield and quality of pyrolysis products, thereby limiting the development of efficient waste-to-energy systems [62,63].

In addition, many studies have employed simplified single-step (typically first-order reaction mechanism) kinetic modelling methods to describe biomass pyrolysis, thereby oversimplifying its inherently multi-component nature. This approach overlooks the multi-component nature of lignocellulosic materials, which comprise hemicellulose, cellulose, and lignin, each decomposing through distinct mechanisms. Hence, this study adopted a multi-stage kinetic modelling approach to better capture the reaction pathways across different temperature regimes and provide comprehensive, localised kinetic and thermodynamic data for Nigeria-derived biomass residues. Additionally, the catalytic influence of mineral and ash content of SD and SB on their pyrolysis was considered to enable more accurate modelling and support the transition from laboratory-scale studies to industrial biorefinery applications.

Thus, this study provides the first location-specific kinetic and thermodynamic data for SD and SB residues from Nigeria, using the Coats–Redfern model to assess their suitability for bioenergy production. It also compares their pyrolysis behaviour with each other and with commonly reported biomasses. To achieve this, the specific objectives include: (1) physicochemical characterisation of the biomass samples to determine their fuel properties, (2) thermal degradation profiling of the biomass samples to investigate their weight loss characteristics across a temperature range from ambient temperature to 900 °C using TGA/DTG curves, (3) estimation of kinetic data, including the activation energy (Ea) and pre-exponential factor (A) for each biomass type by applying the Coats-Redfern integral method, (4) identification of the most appropriate solid-state reaction models that govern the pyrolysis process by statistically evaluating the correlation coefficients (R^2) of various mechanism functions, and (5) derivation of thermodynamic data, including changes in enthalpy (ΔH), Gibbs-free energy (ΔG), and entropy change (ΔS), to assess the energy requirements and spontaneity of the pyrolysis reaction.

The novelty of this study lies in its integrated, location-specific evaluation of the pyrolysis behaviour of two abundant Nigerian waste biomasses (sawdust and sugarcane bagasse). While previous studies on Nigerian biomass largely focused on proximate and ultimate analyses, calorific values, combustion characteristics, and general fuel properties,

detailed investigations of their pyrolysis kinetics, thermodynamic parameters, and reaction mechanisms remain limited. This study bridges this knowledge gap by combining comprehensive physicochemical characterisation [proximate, ultimate, FTIR, SEM, and XRF analyses] with thermogravimetric analysis and a multi-stage Coats–Redfern kinetic approach to determine the activation energy, pre-exponential factor, reaction mechanism, and thermodynamic triplet (ΔH, ΔG, and ΔS). Unlike conventional single-step kinetic analyses, the segmented multi-stage modelling adopted in this work provides a more realistic representation of the distinct decomposition stages of lignocellulosic biomass. The resulting location-specific kinetic and thermodynamic dataset provides valuable design parameters for the development and optimisation of pyrolysis reactors and bioenergy systems utilising Nigerian biomass resources, thereby contributing to the advancement of sustainable waste-to-energy technologies in Sub-Saharan Africa.

2. Materials and Methods

2.1. Materials Collection, Preparation and Characterisation

The study utilised two types of waste biomass: sugarcane bagasse (SB) and sawdust (SD). Dry SB was sourced from farms in Auchi that produce and process industrial cane, while dry SD was collected from a sawmill in Benin City, both within Edo State, Nigeria, during the dry season. Mixed wood waste from Nigerian sawmills and wood industries primarily consists of sawdust, offcuts, and bark from various wood species, often dumped together in an open heap. For this study, sawdust was collected and used for ease of processing. These wastes are usually dumped in a heap outside the processing facilities.

To ensure experimental consistency, the bagasse was pulverised using a hammer mill and sieved using a Glenammer test sieve (200 mm diameter, 30 μm mesh), while the sawdust was also sieved to the same uniform particle size (Figure 1a,b). They were thereafter kept in sealed ziplock bags to prevent moisture from entering prior to analysis.

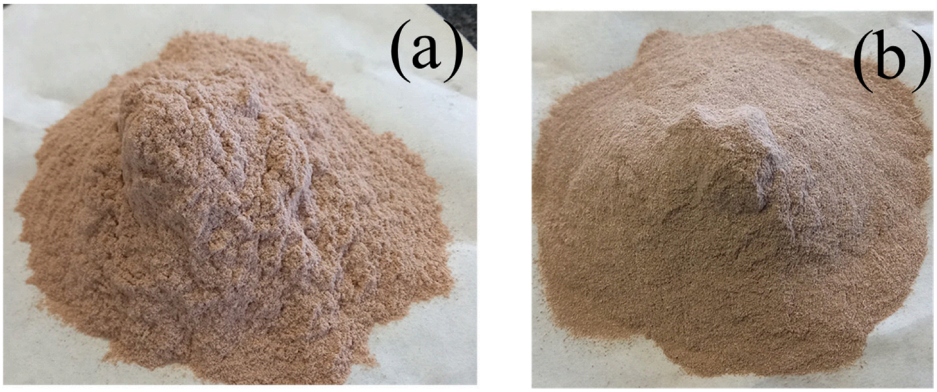


Figure 1. Waste biomass samples (**a**) sawdust and (**b**) sugarcane bagasse.

The proximate properties of the biomass samples were evaluated using a thermogravimetric analyser (NETZSCH-STA449F5, NETZSCH, Wittelsbacherstrase, Germany,) in accordance with ASTM E1131-08. The elemental composition of the samples was evaluated using an Exeter Analytical Organic Elemental Analyser (Model EA1110) in accordance with ASTM D5373-02. Generally, the experiments were replicated three times. The results from the proximate and elemental composition analyses of the biomass samples are shown in Table 1.

Table 1. Proximate and elemental composition analyses of the biomass samples on a dry ash-free basis.

Biomass	Proximate Analysis (wt. %)				Elemental Analysis (wt. %)				
	MC	VM	Ash	* FC	C	H	N	S	* O
SB	3.58 ± 0.25	82.27 ± 0.21	3.31 ± 0.18	10.84 ± 0.20	46.59 ± 0.15	6.52 ± 0.09	3.51 ± 0.25	-	43.38 ± 0.30
SD	4.24 ± 0.15	84.78 ± 0.12	4.45 ± 0.10	6.53 ± 0.12	45.84 ± 0.22	5.87 ± 0.10	3.73 ± 0.22	-	44.56 ± 0.28

$^{*}\,O\% = 100 - (N + C + H + S)\%$; $^{*}\,FC\% = 100 - (MC + VM + ASH)\%$.

The ash composition of the samples was determined using X-ray fluorescence (XRF) spectroscopy (Rigaku RIX-3000, Rigaku Corporation. Akishima, Tokyo, Japan). The results from the ash composition analyses are presented in Table 2.

Table 2. Ash composition analysis for the biomass samples.

Biomass	K_2O	MgO	CaO	Fe_2O_3	Al_2O_3	Cr_2O_3	SiO_2	P_2O_5	SO_3	TiO_2	Cl	ZnO
SB	44.16	0.50	20.40	7.05	0.55	2.36	6.62	1.85	2.50	2.23	9.02	0.87
SD	4.97	0.57	9.01	20.66	2.65	4.11	6.85	1.50	4.93	40.25	1.98	1.13

The morphologies of the biomass samples were analysed using scanning electron microscopy (SEM) with a Tescan Vega 3 microscope(Tescan, Brno, Czech Republic). The biomass samples were mounted on aluminium stubs using sticky carbon tape, coated with a thin layer of gold, and thereafter vacuum-dried and scanned at an acceleration voltage of 20 kV. The surface functional groups of the samples were analysed by Fourier transform infrared (FTIR) spectroscopy on a ThermoFisher Scientific iS50 FTIR spectrometer (ThermoFisher Scientific, Maddison, WI, USA.), with scans from 4000 to 400 cm^{-1} at a resolution of 4 cm^{-1} and a scanning speed of 2 mm/s. The briquettes were ground to a fine powder before FTIR analysis.

2.2. Thermogravimetric Analysis

To evaluate the thermal degradation behaviour of the two biomass samples, a thermogravimetric analyser (NETZSCH-STA449F5) (Figure 2) was used to analyse their thermochemical conversion at a single heating rate of 20 °C/min in an inert nitrogen atmosphere, flowing at 40 mL/min. A previous study indicated that at this heating rate, the degradation of the biomass materials occurs in a shorter time; however, the data quality remains high with few outliers [13]. About 12 ± 0.5 mg of biomass was weighed and heated from ambient temperature to 900 °C under the specified conditions. The data obtained were used to generate TG and DTG curves for all samples.

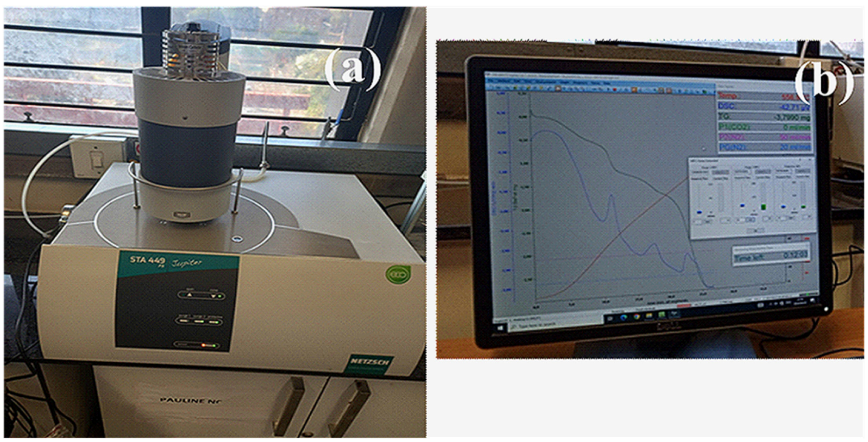


Figure 2. Setup for the thermogravimetric analysis. (**a**) NETZSCH = STA449 F5 TGA, (**b**) computer monitor.

2.3. Analysis of Pyrolysis Performance

The efficiency of a pyrolysis process can be evaluated using various parameters, including the initial and final decomposition temperatures, T_i and T_f, respectively; peak temperature (T_p); maximum decomposition rate $(dw/dT)_{max}$; average decomposition rate $(dw/dT)_{av}$, comprehensive pyrolysis index (*CPi*), devolatilisation index (*Di*), pyrolysis stability index (*Pi*) and the overall mean reactivity (MRo) [64]. The initial decomposition temperature (T_i) was determined using the intersection method by extrapolating the onset of the partial peak associated with hemicellulose decomposition.

2.3.1. Comprehensive Pyrolysis Index

The comprehensive pyrolysis index (*CPi*) is an essential indicator of the overall performance of the pyrolysis process, and it offers an inkling for achieving higher efficiency and yield [65,66]. An increase in the *CPi* signifies a more efficient process characterised by rapid degradation and significant weight loss, leaving little residual waste [67,68]. It is determined using Equation (1) [69].

$$CPi = \frac{-(dw/dT)_{\max} \times -(dw/dT)_{av} \times wf}{T_i \times T_{p,\max} \times \Delta T_{1/2}} \quad (1)$$

where $\Delta T_{1/2}$ is the temperature difference at the middle of the curve with the highest peak; w_f is the difference between the initial and final weights of the biomass sample; and $T_{p,max}$ is the maximum temperature.

2.3.2. Devolatilisation Index

The deoxygenation index (*Di*) describes the effectiveness of the release of volatile matter (VM) from the biomass during pyrolysis [62]. A high *Di* value shows rapid devolatilisation, which is essential for maximum outputs [24]. As a result, the *Di* is a crucial parameter for optimising pyrolysis, especially when the aim is to produce specific fractions in optimal amounts, e.g., bio-oil or biochar. It was calculated using Equation (2) [69].

$$Di = \frac{(dw/dT)_{\max}}{T_i \times T_{p,\max} \times \Delta T_{1/2}} \quad (2)$$

2.3.3. Pyrolysis Stability Index

The pyrolysis stability index (*Pi*) is used to quantify the predictability of a material to decompose over time and temperature [64]. An increase in *Pi* implies a more predictable process, which is critical in scaling an industry; reliable yields and the ability to manage and optimise the system are guaranteed [70]. The operators can generate a more consistent, high-quality product by helping minimise fluctuations in the process; thus, the *Pi* is one of the most critical metrics to create strong and commercially viable pyrolysis operations [65,71]. Equation (3) [64] was used to compute the *Pi.*

$$Pi = \frac{-(dw/dT)_{\max}}{T_i \times T_{p,\max}} \times 8.586 \times 10^7 \quad (3)$$

2.3.4. Mean Reactivity

One of the most basic measures to determine the reaction behaviour of biomass during pyrolysis is the Mean Reactivity (*MR*) [72]. By computing the Overall Mean Reactivity (MRo), the sum of the MR values for all peaks in the DTG curves, researchers can estimate the decomposition rate and temperature [72]. High MRo values indicate a highly reactive substance that dissolves readily at low temperatures [64]. This quality especially helps maximise throughput and efficiency, as reactive feedstocks are readily converted into

products. Additionally, high reactivity permits lower operating temperatures, which can greatly reduce energy requirements and enhance overall process operation [69]. It was determined using Equation (4) [69].

$$MRo = 100 \sum \frac{(dw/dT)\max}{Tp} \quad (4)$$

2.4. Kinetic Modelling

Kinetic modelling plays an important role in understanding the thermal decomposition behaviour of biomass during pyrolysis. In this study, the Coats-Redfern integral method was employed to determine the kinetic parameters from the TGA data. According to Vyazovkin and Muravyev [73], single-heating-rate methods such as the Coats-Redfern model present some challenges in the analysis of kinetic triplets for complex biomass systems. Nevertheless, the method remains useful for preliminary comparative analyses under identical conditions and was adopted in this study for practical reasons. First, the estimated kinetic parameters are adequate for comparing biomass behaviour under the same experimental conditions. Second, multi-heating-rate methods are time- and resource-intensive, requiring advanced equipment and expertise. Third, single-heating-rate experiments better reflect the constant-heating conditions commonly applied in practical pyrolysis systems, thereby improving the applicability of the results. Therefore, despite its limitations, the Coats-Redfern method remains a practical and reliable approach when interpreted carefully [20,21,74–76].

The rate constant of the reaction (k) is dependent on the absolute temperature (T), and the method is described by the Arrhenius equation [77].

$$k(T) = Ae^{-\frac{Ea}{RT}} \quad (5)$$

T indicates the temperature (K), A signifies the pre-exponential factor (min^{-1}), E_a indicates the activation energy (kJ/mol), and R is the universal gas constant (0.008314 kJ/mol K). The rate of reaction between solid and gas is delineated by Equation (6) [77]:

$$\frac{dx}{dt} = k(T) \cdot g(x) \quad (6)$$

dx/dt represents the rate of decomposition, which is linearly dependent on the rate constant. x represents the biomass weight loss ratio during pyrolysis, t signifies the time for the pyrolysis, and $g(x)$ is the differential form of the reaction model, which depends on the reaction mechanism. The weight loss ratio (x) can be obtained from thermogravimetric analysis data, as follows [78]:

$$x = \frac{m_o - m_t}{m_o - m_f} \quad (7)$$

m_0, m_t, and m_f are the initial, instantaneous, and residual mass of samples during the pyrolysis process, respectively.

Combining Equations (5) and (6) at the heating rate ($\beta = dT/dt$) and rearranging gives Equation (8):

$$\frac{dx}{dT} = \frac{A}{\beta} e^{-\frac{Ea}{RT}} \times g(x) \quad (8)$$

The integral expression of $g(x)$ is presented in Equation (9).

$$f(x) = \int_0^x \frac{dx}{g(x)} = \frac{A}{\beta} \int_{To}^{T} e^{-\frac{Ea}{RT}} dT \quad (9)$$

A = preexponential factor in per minute, E_a = activation energy in kJ/mol, $k(T)$ = rate constant, R = universal gas constant, T = the reaction temperature (K), x = conversion rate and $g(x)$ = kinetic model, $f(x)$ = the integral form of the kinetic model.

Kinetic parameters, like the activation energy and the preexponential factors, can be estimated by integrating Equation (9) and applying a mathematical approximation for the exponential term. For the Coats-Redfern method, after approximation and rearrangement, the solution is expressed as Equation (10) [78]:

$$\ln \frac{f(x)}{T^2} = \ln \frac{AR}{\beta E_a} - \frac{E_a}{RT} \quad (10)$$

Straight lines can be fitted to the plots of $\ln[f(x)/T^2]$ against $1/T$, and the activation energy (E_a) is estimated from the slope ($-E_a/R$) of the plots, while the pre-exponential factor (A) is determined from the intercept $\ln [AR/\beta E_a]$ of the plots.

In this study, to increase the accuracy and completeness of the kinetic analysis, eight different reaction mechanism functions [$f(x)$] were utilised. These functions represent various kinetic models, including those based on reaction order, diffusion control, and contracting spheres, and are detailed in Table 3.

Table 3. Reaction models commonly used to assess the biomass degradation mechanism [79,80].

Reaction Model	Reaction Mechanism	Code	$g(x)$	$f(x)$
Order-based	1st order	R1	$1-x$	$-\ln(1-x)$
	2nd order	R2	$(1-x)^2$	$(1-x)^{-1}-1$
	3rd order	R3	$(1-x)^3$	$1/2[(1-x)^{-2}-1]$
Diffusion-based	1-D diffusion (Parabolic Rule)	D4	$(2x)^{-1}$	x^2
	2-D diffusion (Valensi equation)	D5	$[-\ln(1-x)]^{-1}$	$(1-x)\ln(1-x)+x$
	3-D diffusion (Ginstling-Brounshtein)	D6	$3/2[(1-x)^{1/3}-1]^{-1}$	$1-2/3x-(1-x)^{2/3}$
Contracting sphere-based	Contracting sphere area	C7	$2(1-x)^{1/2}$	$1-(1-x)^{1/2}$
	Contracting sphere volume	C8	$3(1-x)^{2/3}$	$1-(1-x)^{1/3}$

2.5. Activation Thermodynamic Analysis

The activation thermodynamic triplets: change in enthalpy (ΔH*), change in Gibbs free energy (ΔG*), and change in entropy (ΔS*), provide insight into the kinetics (speed) of the thermal decomposition reaction. Analysing these parameters enables optimisation of pyrolysis conditions to enhance energy efficiency, improve overall process performance, and increase product yield. The calculations utilise fundamental constants, including the Boltzmann constant (K_B = 1.381 × 10^{-23} J/K), Planck's constant (h = 6.626 × 10^{-34} J·s), the gas constant (R = 8.314 J/mol·K), and the DTG peak temperatures (T_p in Kelvin) of each reaction stage [66,81–83].

In pyrolysis studies, ΔH* represents the energy needed to commence biomass thermal degradation. It was calculated using Equation (11).

$$\Delta H^* = E_a - RT_p \quad (11)$$

where R = universal gas constant, T_p = peak temperature of each stage, and E_a = activation energy.

A change in Gibbs free energy (ΔG*) indicates the total amount of reversible work a system can perform under the operating conditions. It was estimated using Equation (12).

$$\Delta G^* = E_a + RT_p \ln\left(\frac{k_B T_p}{hA}\right) \quad (12)$$

Entropy change (ΔS*) measures the level of order or randomness within the system as the pyrolysis proceeds, and its value was calculated following Equation (13).

$$\Delta S^* = \frac{\Delta H - \Delta G}{T_p} \quad (13)$$

2.6. Multi-Stage Segmented and Generic Single-Step Methods

This section evaluates two kinetic modelling methods for biomass pyrolysis: the generic single-stage and the multi-stage segmented methods. The segmented method provides a granular perspective by assigning unique kinetic parameters to individual temperature intervals, whereas the single-stage model treats the whole process as a uniform reaction having consistent properties throughout the heating span [84].

Multi-Stage Segmented Approach

The multi-stage segmented model considers the distinct phases of the pyrolysis process, delineated by specific temperature spans, as individual single-step reactions with their own kinetic constants [85,86]. This technique accounts for the shift in dominant reaction pathways throughout the process, enabling a better accurate depiction of the decomposition process within each interval [87]. To establish comprehensive kinetic data over the entire temperature span, results from each segment were combined by deploying the weighted average approach:

i. Contribution from each stage

The weight loss (w_i) for each stage was determined by the stage's relative contribution to the overall weight loss, as defined in Equation (14).

$$wi = \frac{\Delta xi}{\Delta xtotal} \quad (14)$$

ii. Compute the total activation energy ($E_{a,total}$)

The total activation energy was calculated using Equation (15).

$$E_{a,total} = \sum_{i=1}^{n} wiEa,i \quad (15)$$

where $E_{a,i}$ = activation energy for each stage.

iii. Total preexponential factor (A_{total})

The total preexponential factor was calculated using a logarithmic average as shown in Equation (16).

$$A_{total} = \exp\left(\sum_{i=1}^{n} wi \ln Ai\right) \quad (16)$$

where A_i = pre-exponential factor for each stage.

The multi-stage segmented method is based on the weighted average of the activation energies (*Ea*,*i*) across various temperature intervals, rather than a simple average. This guarantees that the influences of segments that have lost the most weight have a corresponding higher impact on the overall kinetic values [88]. On the other hand, the generic

single-stage approach treats the entire pyrolysis process as a single, holistic reaction. It simplifies the kinetic analysis by assuming a single dominant pathway with a universal activation energy (Ea,u) and a pre-exponential factor (*Au*). This simplified representation is especially useful with large-scale usage or at the preliminary design stages, where a simplified model is more cost-effective [89,90].

3. Results

3.1. Thermal Analysis

Figures 3 and 4, respectively, were the results of thermal decomposition of the biomass studied (sawdust and sugarcane bagasse) using thermogravimetric analysis (TGA) and derivative thermogravimetry (DTG). Table 4 shows key parameters of the analysis.

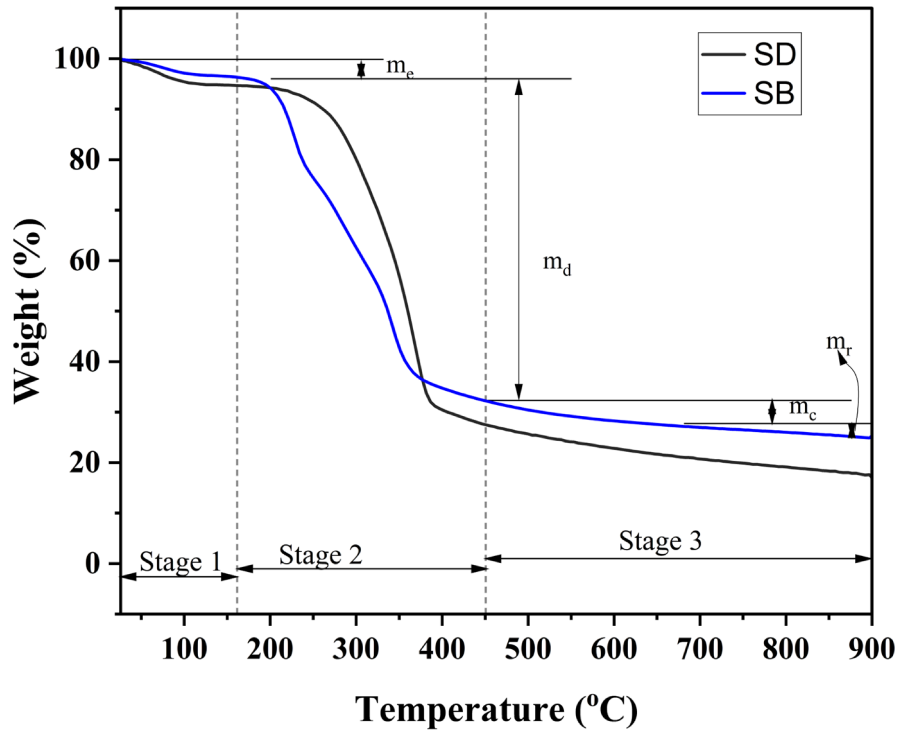


Figure 3. TGA profiles indicating weight loss on the studied samples during thermal decomposition. m_e, m_d, and m_c denote the weight loss during drying, devolatilisation, and char formation, respectively, while m_r denotes the residual weight.

Table 4. Key parameters during the pyrolysis stages of the biomass samples.

Feedstock	Decomposition Stages	Initial Temp (°C)	Final Temp (°C)	Peak Temp (°C)	Weight Loss (%)	$(\frac{dw}{dT})_{max}$ (%/°C)	$(\frac{dw}{dT})_{mean}$ (%/°C)	Fractional Weight (w_i)
Sawdust	Stage 1: drying	25	166	57	6.38	−0.07	−0.03	0.082
	Stage 2: devolatilisation	166	451	351	66.12	−0.68	−0.28	0.791
	Stage 3: char formation	451	900	-	10.14	−0.04	−0.01	0.128
Sugarcane bagasse	Stage 1: drying	25	168	76	4.23	−0.05	−0.02	0.056
	Stage 2: devolatilisation	168	450	227, 287, 341	63.53	−0.31, −0.53, −0.58	−0.12, −0.20, −0.22	0.852
	Stage 3: char formation	450	900	-	8.10	−0.02	−0.005	0.092

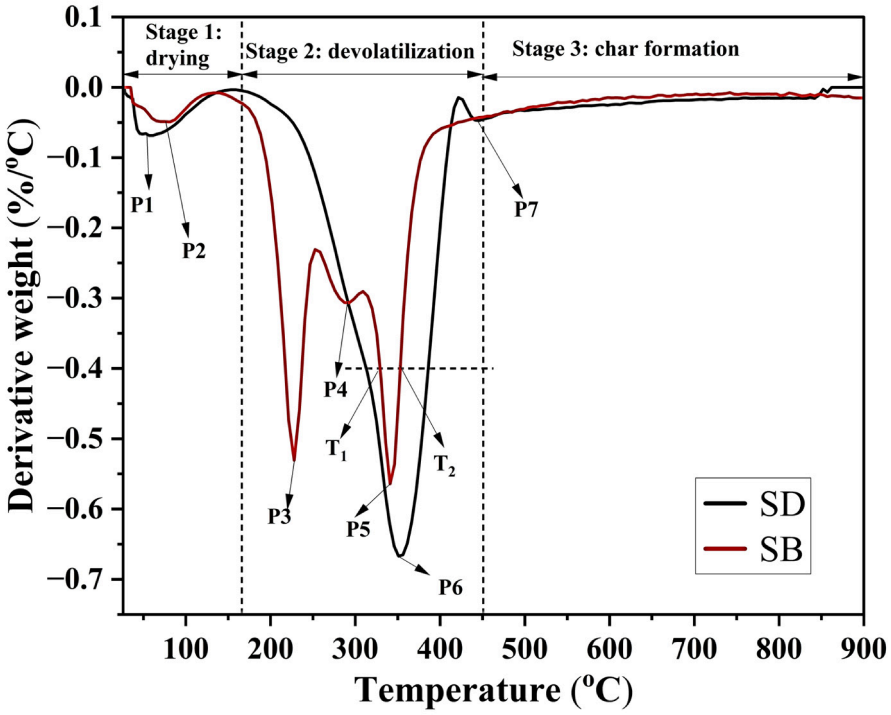


Figure 4. DTG profiles indicating the decomposition rate for the studied samples. (P1–P2): peaks at stage 1, (P3–P7): peaks at stage 2, T_1: lower temperature at the middle of the peak decomposition rate, T_2: upper temperature at the middle of the peak decomposition rate.

3.1.1. Drying

The provided DTG curves for sawdust and sugarcane bagasse reveal valuable insights into the behaviour of both biomasses during thermal decomposition. The process of decomposition can be broken down into various key stages, each of which is related to the main components: moisture, hemicellulose, cellulose, and lignin. This first, low-weight-loss peak, at about 76 °C for sugarcane bagasse and 57 °C for sawdust, is largely due to the loss of inherent and surface moisture and of lighter volatile compounds in the biomass. This is the dehydration phase, and it was found that the dehydration occurred between 25 and 168 °C for sugarcane bagasse and between 25 and 166 °C for sawdust.

3.1.2. Devolatilisation Stage

This is the most active stage, during which the main components of biomass (hemicellulose and cellulose) decompose, releasing volatiles. For the sugarcane bagasse, there are two prominent peaks in the DTG plot between 200 and 350 °C. The initial minor peak observed between 200 and 250 °C is likely due to the thermal decomposition of hemicellulose, which typically occurs between 200 and 300 °C [15,91,92]. This is the stage at which hemicellulosic components are broken down into volatile compounds, resulting in a sharp negative peak in the DTG curve. The peak at higher temperatures, 300–350 °C, suggests the breakdown of cellulose, which occurs in this temperature range [15,93]. This is associated with the depolymerisation of cellulose chains and the release of volatiles. This peak is higher and sharper than the hemicellulose peak because cellulose has a more ordered, crystalline structure, which facilitates faster, more uniform decomposition over a specific temperature range [94]. In the case of sawdust, the steep downward curve at around 350 °C is an indication of an important decomposition stage, which is characteristic of lignocellulosic biomass, reflecting the decomposition of hemicellulose and cellulose [95–97]. The steepness of this peak indicates a fairly homogeneous process of decomposition of these components.

Additionally, the magnitude of the peaks in the DTG curve indicates the relative abundance and thermal stability of these components. The higher intensity of the cellulose degradation peak suggests a significant cellulose content in the biomass sample, aligning with compositional analyses reported in recent literature [98]. The SB curve is shifted to the left compared to SD, indicating that sugarcane bagasse begins decomposing at lower temperatures than sawdust. SD exhibits higher peak magnitude, indicating more intense devolatilisation processes, whereas SB's peaks are slightly shifted and less intense, suggesting differences in composition or thermal stability.

Recent studies corroborate these observations. For instance, Bahú, et al. [91] and Najafi, et al. [15] reported similar DTG profiles for sugarcane bagasse, with peaks at approximately 220 °C and 340 °C corresponding to the degradation of hemicellulose and cellulose, respectively. Likewise, El-Naggar, et al. [93] observed comparable thermal degradation behaviour in sugarcane bagasse, emphasising the multi-stage nature of biomass pyrolysis. Guida, et al. [95] studied the thermal degradation of sawdust at different heating rates and reported major decomposition peaks around 300 to 340 °C, attributed primarily to hemicellulose and cellulose. Similarly, Mishra and Mohanty [96] observed a comparable DTG profile for sawdust, emphasising the dominant degradation within 300–350 °C, with a broad lignin degradation phase extending beyond 500 °C.

3.1.3. Char Formation Stage

This phase occurs between 450 and 900 °C. It is the gradual decomposition of lignin, which is extremely complex and thermally stable, that leads to the formation of a carbonaceous residue (char). There is no sharp peak in this phase since lignin decomposes more slowly over a broad temperature range than the other components [98–100]. The fact that the curves converged to a zero weight-loss rate indicates the stabilisation of the remaining char and ash.

3.2. FTIR Spectroscopy Results

Figure 5 presents the FTIR spectra of sawdust (SD) and sugarcane bagasse (SB), which are typical of lignocellulosic biomass mainly composed of cellulose, hemicellulose, and lignin [98,101]. Although the chemical fingerprints of the two samples are almost identical, the absorption intensity (deeper transmittance dips) of the SB spectrum is much greater than that of the SD spectrum, suggesting a higher concentration of functional groups.

The significant peaks in Figure 5 reflect the chemical environments delineated in the preceding paragraphs [98,101,102]. The broad, strong band at 3600–3200 cm^{-1} is attributed to the stretching vibrations of the hydroxyl (O-H) groups. They occur in the cellulose and hemicellulose chains, as well as in the phenolic groups of lignin and absorbed water. The broadness shows that there is a lot of hydrogen bonding. The steep peak at around 2910 cm^{-1} is due to the C-H stretching of aliphatic groups (CH_2 and CH_3) in cellulose and hemicellulose. The C=O stretching of acetyl and ester groups, typical of hemicellulose, is responsible for the peak around 1700 cm^{-1}. The region near 1600 cm^{-1} corresponds to aromatic C=C skeletal vibrations from the lignin component. The band between 1200 and 1000 cm^{-1} is the most intense region of the spectrum, often referred to as the carbohydrate region. The steep peak at about 1030 cm^{-1} is suggestive of a C-O stretching vibration, characteristic of carbohydrates such as cellulose and hemicellulose.

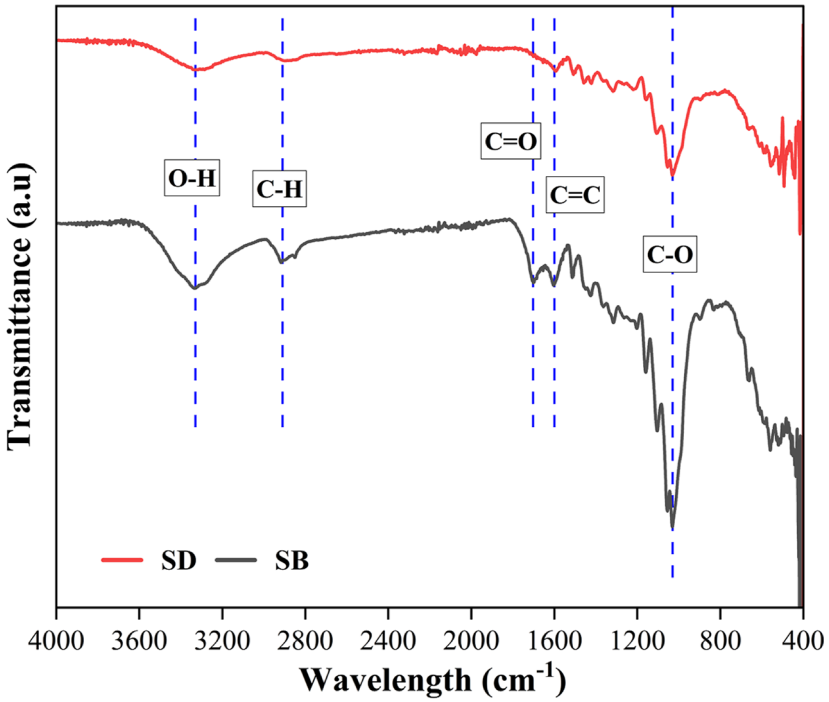


Figure 5. FTIR spectra of the studied biomass samples: sawdust (SD) and sugarcane bagasse (SB).

Figure 5 shows that the peaks are almost identical for both biomass samples, suggesting they are chemically similar. The two studied biomasses can be used as viable feedstocks for bioenergy applications, as they have the same structural polymers. The peaks of sugarcane bagasse (SB) are much lower than those of sawdust (SD), particularly at 1030 and 3300 cm^{-1}. This indicates that, for the same sample thickness or concentration, SB has a higher density of functional groups, probably due to a higher relative content of cellulose and hemicellulose than in sawdust.

3.3. Analysis of SEM Micrographs of the Biomass Samples

Figure 6 shows the SEM micrographs of the studied biomass (sawdust and sugarcane bagasse) at a magnification of 1.00 kx. The SEM micrographs provide detailed insights into their surface morphology, which plays a crucial role in their behaviour during pyrolysis.

In Figure 6, the sawdust (SD) micrograph shows highly organised, elongated, and relatively smooth fibre bundles, with a loose arrangement, displaying clean fractures and separated, thin microfibrils. During pyrolysis, heat travels through the thick cell walls, which directly influence how heat and mass transfer occur during thermal decomposition. The smooth, open fibrous channels in SD allow the even transfer of heat, leading to easy escape of volatiles during devolatilisation, resulting in lower char yield [103,104]. The sugarcane bagasse (SB) micrograph reveals a highly porous and packed structure. This dense and clustered matrix traps heavy volatile fragments inside the compact structure, promoting secondary char-forming re-polymerisation reactions, which is likely responsible for the higher char yield observed in SB [105].

Notably, while the FTIR spectra confirm that both biomass materials have the necessary chemical precursors (cellulose, hemicellulose, and lignin) for bioenergy applications, the SEM micrographs show that the dense packing in SB structurally supports the carbon skeleton as it carbonises through the char formation stage, preventing the complete breakdown and volatilisation experienced by the loose fibres of SD. This indicates that sawdust will be physically superior for processes requiring rapid heat transfer, such as fast pyrolysis,

while sugarcane bagasse will be better suited to slow pyrolysis or carbonisation, where high-quality biochar is the desired end-product.

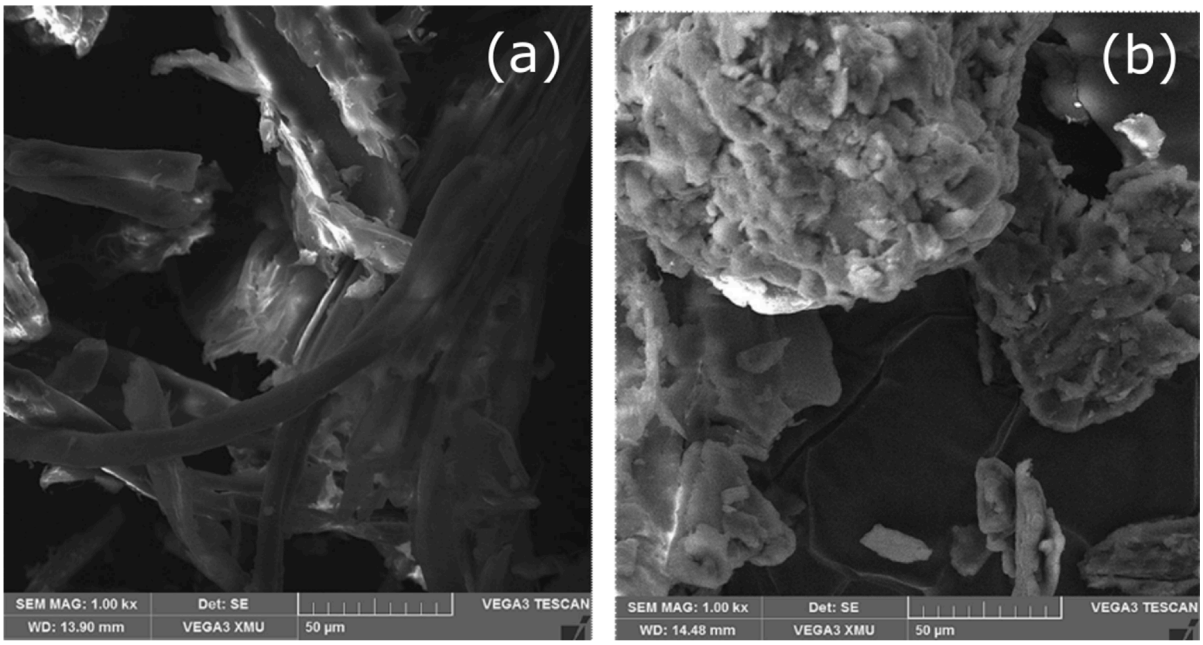


Figure 6. SEM micrographs of the studied biomass: (**a**) sawdust and (**b**) sugarcane bagasse.

3.4. Pyrolysis Parameters

Pyrolysis metrics offer essential perspectives on how different biomass types break down under heat [64]. Vital indices, specifically overall mean reactivity (*MRo*), the comprehensive pyrolysis index (*CPi*), the devolatilisation index (*Di*), and the pyrolysis stability index (*Pi*), have been calculated and are summarised in Table 5. A thorough understanding of these properties is vital for refining pyrolysis operations and enhancing biomass-to-bioenergy and biochar conversion.

Table 5. Pyrolysis parameters for the studied biomass samples.

Parameters	Sawdust (SD)	Sugarcane Bagasse (SB)
Initial devolatilisation temperature (T_i, °C)	166	168
Peak temperature (T_p, °C)	351	341
Final devolatilisation temperature (T_f, °C)	451	450
Weight loss during the entire pyrolysis process (%)	82.64	75.86
Residual weight (m_r, %)	17.36	24.15
$-(dw/dT)_{max}$ (%/°C)	0.68	0.58
$-(dw/dT)_{mean}$ (%/°C)	0.28	0.22
Initial temperature at the midpoint of maximum combustion rate (T_1, °C)	298	331
Final temperature at the midpoint of maximum combustion rate (T_2, °C)	392	351
Midpoint temperature range ($\Delta T_{1/2}$, °C)	94	20
Mean reactivity during stage 1 (%/°C)	0.1228	0.0658
Mean reactivity during stage 2 (%/°C)	0.1937	0.1701
Mean reactivity during stage 3 (%/°C)	0.0059	0.0029
Overall mean reactivity (%/°C)	0.3224	0.2388
Pyrolysis stability index (%/°C^2)	1002.0389	869.2711
Devolatilisation index (10^{-7}, %/°C^3)	1.2416	5.0621
Comprehensive pyrolysis index (10^{-6}, $\%^3$/°C^3)	3.4885	3.4583

The mean reactivity (MR) data for the various stages provide insights into how rapidly biomass materials lose mass as a function of temperature. Sawdust (SD) exhibits higher mean reactivity in all the stages, indicating faster decomposition rates across the three

stages. However, the highest mean reactivity was observed during stage 2 for both biomass materials, signifying that stage 2 is the most active stage during their pyrolysis. SD exhibits a higher overall mean reactivity, likely stemming from its elevated volatile content, accelerated breakdown speeds, a highly reactive lignocellulosic framework, and high metal oxide (Fe_2O_3) content, which synergistically accelerated its thermal decomposition during pyrolysis [87,106–108]. This indicates that SD decomposes more readily under pyrolysis conditions, aligning with its DTG curve, which shows broader peaks, suggesting a more uniform, slower devolatilisation process, yet with a higher total reactivity index.

The devolatilisation index measures the extent of volatile release during pyrolysis; higher values indicate more intense devolatilisation.SB exhibits a significantly higher devolatilization index (5.0621×10^{-7}%/°C^3), indicating it releases more volatiles more rapidly. Interestingly, SB shows a significantly higher *Di* value despite lower overall reactivity, likely due to its highly porous structure and specific hemicellulose types that allow for a sudden, high-volume release of light volatiles early in the heating process [106,108,109]. In addition, SB contains a significant amount of K_2O, a potent catalyst that lowers the thermal decomposition temperature of cellulose and hemicellulose [110,111], contributing to SB's higher devolatilisation index. Conversely, SD exhibited a lower devolatilization value compared to SB, probably due to its smooth, parallel fibrous microstructure, which allows heat to distribute evenly, causing components to break down sequentially rather than all at once [104].

The pyrolysis stability index reflects the material's resistance to rapid decomposition; higher values generally denote better pyrolysis performance rather than resistance in a restrictive sense [112], indicating greater stability. It measures the intensity of the mass loss rate relative to the peak temperature. SD exhibits a higher stability index (1002.04%/°C^2) than SB (869.27%/°C^2), indicating it is more thermally stable and decomposes more gradually. This suggests that SD releases volatiles more effectively once the ignition temperature is reached and maintains thermal integrity over a broader temperature range [64]. Hence, SD's DTG curve peaks are broader, indicating gradual devolatilisation. Conversely, SB shows a lower pyrolysis stability index, which may be attributed to its higher devolatilisation index.

The comprehensive pyrolysis index combines aspects of reactivity, stability, and devolatilization to provide an overall measure of pyrolysis behaviour. Because SD (3.4885×10^{-6}, %^{3}/°C^3) has a slightly higher comprehensive pyrolysis index than SB (3.4583×10^{-6}, %^{3}/°C^3), it is marginally more reactive overall, though both materials are highly competitive. The slight edge in SD's index means it possesses better thermal volatility and ignition characteristics under pyrolytic conditions.

In summary, sugarcane bagasse (SB) exhibits higher devolatilization, indicating rapid volatile release. However, its dense and packed granular matrix traps these rapidly released volatiles internally, resulting in a higher final char yield. In contrast, sawdust (SD) shows higher stability and broader decomposition peaks, confirming its superior overall thermal reactivity and sequential, highly stable, and predictable mass loss, making it an ideal candidate for high-yield bio-oil production. These differences highlight the distinct pyrolysis behaviours and potential applications of the studied biomass, influenced by their thermal properties and specific compositions.

3.5. Kinetic Analysis

Model fitting is a fundamental tool for analysing pyrolysis data. It enables the evaluation of biomass kinetic parameters and emphasises their differences. By applying experimental data to several reaction models, crucial parameters were identified, shedding light on the thermal decomposition of the investigated biomass samples. The multi-stage approach, including stages 1 (dehydration; 25 °C to Ti), 2 (devolatilisation; Ti to Tf), and

3 (char-formation; T_f to 900 °C), and the single-stage approach (25 to 900 °C) were considered. To determine the reaction model best suited for each stage (multi-stage approach) and across the entire temperature range (single-stage approach) of the biomass pyrolysis process, the Coats-Redfern method was applied to thermogravimetric analysis data, and the goodness-of-fit of the various reaction models was evaluated. To evaluate how well the different reaction models aligned with the data, the coefficient of determination (R^2) was calculated at every pyrolysis stage, and residual analysis was performed to minimise errors between predicted and experimental values. The obtained results from each model are summarised in Table 6.

Table 6. Kinetic parameters for the studied biomass.

Decomposition Stages/Reaction Models	Ea (kJ/mol)	A (min^{-1})	R^2	Ea (kJ/mol)	A (min^{-1})	R^2
	Sawdust			Sugarcane Bagasse		
Drying stage: (25 °C to T_i)						
R1	12.0563	0.3051	0.6547	22.9019	14.2667	0.7927
R2	12.3809	0.3473	0.6619	23.1160	1.9708×10^8	0.7757
R3	12.5593	0.3911	0.6690	23.3320	17.2683	0.7987
D4	29.8525	6.9271	0.7537	51.3309	6.741×10^3	0.8312
D5	30.0157	3.7253	0.7551	51.4718	3.576×10^3	0.8319
D6	30.0706	0.8484	0.7556	51.5190	8.10×10^2	0.8322
C7	11.9326	0.1435	0.6511	22.79019	6.8022	0.7912
C8	11.9738	0.0976	0.6523	22.8309	4.6079	0.7917
Devolatilisation stage: (T_i to T_f)						
R1	40.8936	4.85×10^2	0.9659	28.7589	55.3914	0.9365
R2	59.9387	5.194×10^4	0.9600	45.2313	4.966×10^3	0.9831
R3	83.5396	1.438×10^7	0.9411	65.9541	1.133×10^6	0.9775
D4	64.3582	1.994×10^4	0.9546	44.4504	6.03×10^2	0.8573
D5	71.9119	6.284×10^4	0.9634	50.4739	1.568×10^3	0.8941
D6	75.0613	2.982×10^4	0.9663	53.0715	7.00×10^2	0.9078
C7	33.3823	36.1076	0.9564	22.4767	4.5520	0.8725
C8	35.7362	43.9925	0.9608	24.4249	5.3574	0.8974
Char formation stage: (T_f) to 900 °C						
R1	3.4695	0.0445	0.8833	3.0818	0.0476	0.7263
R2	23.0714	25.2984	0.8116	38.8038	7.45×10^2	0.7179
R3	57.7232	3.022×10^5	0.8617	1.03×10^2	2.576×10^8	0.7391
D4	11.2907	0.1178	0.9774	12.3144	0.1551	0.9779
D5	8.5311	0.0549	0.9779	9.3832	0.0789	0.9856
D6	6.1574	0.0084	0.9412	7.0417	0.0129	0.9754
C7	9.8527	0.0740	0.9596	10.0389	0.0884	0.9689
C8	7.9345	0.0379	0.9288	7.0444	0.0346	0.9575
Total (based on multistage)	62.8999	1.225×10^3		42.2705	1.046×10^3	
Full range temperature (25 °C to 900 °C); based on global single-stage approach						
R1	13.9657	0.7173	0.8829	17.9492	2.4021	0.9076
R2	23.0938	21.4873	0.9151	29.3732	1.53×10^2	0.9626
R3	34.7299	1.277×10^3	0.8743	45.8162	4.261×10^4	0.8796
D4	26.2386	2.3045	0.8723	31.6096	7.9858	0.8321
D5	28.9202	3.0716	0.8940	35.4489	15.4512	0.8760
D6	30.0670	1.0339	0.9026	36.6644	5.3536	0.8887
C7	10.7991	0.1001	0.8024	14.2314	0.2829	0.8029
C8	11.7473	0.0986	0.8337	14.9772	0.2579	0.8344

T_i = initial devolatilization temperature, T_f = final devolatilization temperature.

To ensure the kinetic parameters precisely represented the biomass's thermal behaviour, the model exhibiting the highest R^2 and lowest residuals was chosen for each stage [64]. This selection process provided a clearer understanding of the specific kinetics involved in each phase of decomposition. At each stage and across the entire temperature

span, distinct linear-fitting patterns were observed; for example, Figures 7 and 8 compare the various integral models applied over the full range of 25 °C to 900 °C.

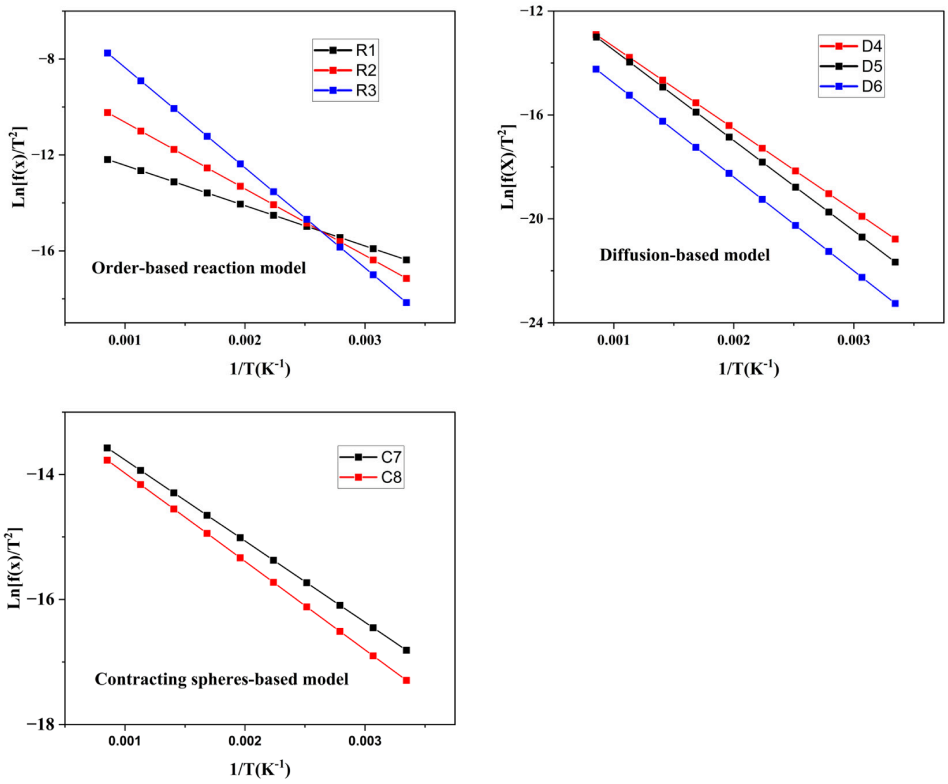


Figure 7. Linear plots derived from the integral method for determining the kinetic parameters of sawdust across the entire temperature span (25 °C to 900 °C).

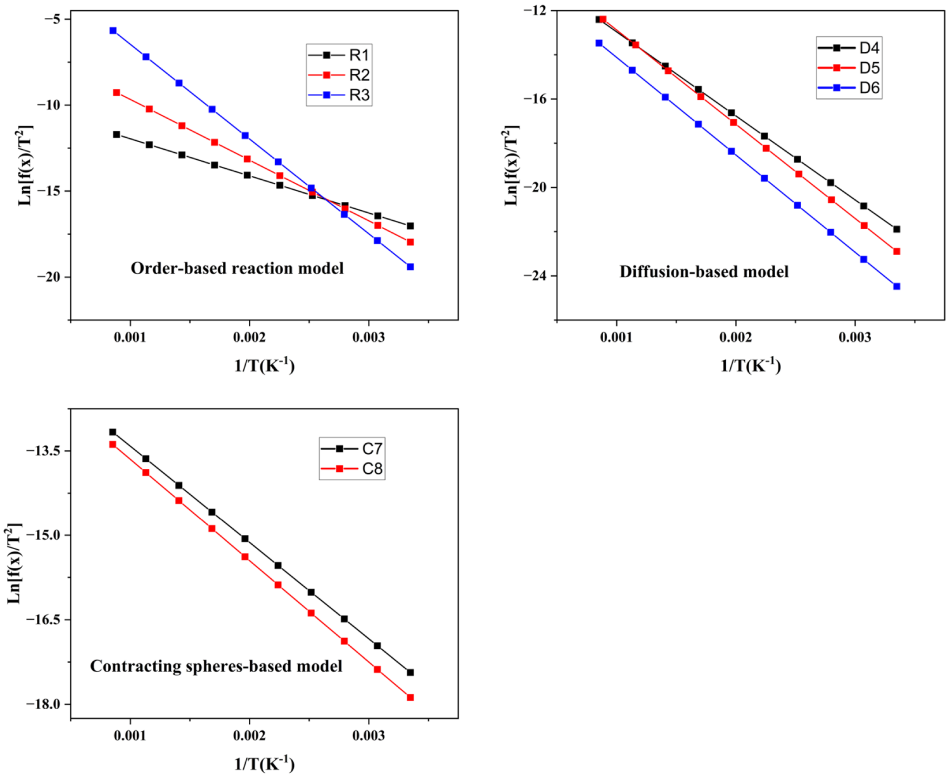


Figure 8. Linear plots derived from the integral method for determining the kinetic parameters of sugarcane bagasse across the entire temperature span (25 °C to 900 °C).

Best Fit Models for SD and SB

Table 6 presents the kinetics of the thermal decomposition of both sawdust (SD) and sugarcane bagasse (SB) under the multi-stage and global single-stage (full-temperature range) approaches. Evaluating kinetic data across discrete decomposition stages and temperature intervals offers a better comprehension of biomass pyrolysis. The multi-stage process comprises drying (stage 1: 25 °C to T_i), devolatilization (stage 2: T_i to T_f), the active pyrolysis stage, and char formation (stage 3: T_f to 900 °C), each governed by distinct kinetic behaviours. The overall temperature span (25 to 900 °C) analysis treats these stages as a single unit and presents a holistic overview of the thermal decomposition of the biomass materials. The variation in activation energy (Ea), pre-exponential factor (A), and correlation coefficient (R^2) across stages confirms that biomass decomposition is mechanistically heterogeneous, and model selection must be stage-specific for meaningful interpretation.

In the drying stage, both biomasses exhibit relatively low activation energies, indicating that this phase primarily involves moisture removal rather than chemical bond breaking. Sawdust shows lower Ea values (~12–30 kJ/mol) compared to sugarcane bagasse (~23–51 kJ/mol), indicating that water is weakly bound in sawdust. This difference can be attributed to the more fibrous and heterogeneous structure of bagasse, which enhances moisture retention through hydrogen bonding and capillary effects [113,114]. The diffusion-based model D6 provides the best fit for both biomasses at this stage, as reflected in their higher R^2 values (0.7556 for SD and 0.8322 for SB), indicating that internal moisture transport plays a dominant role during drying. This observation is consistent with studies showing that biomass drying is predominantly moisture-transfer-limited and controlled by internal diffusion and mass transfer processes within the porous structure, rather than by chemical reaction kinetics [115]. Nevertheless, the relatively low R^2 values (~0.65–0.83) suggest limited model reliability in this region. This deviation is expected, as drying behaviour is governed by combined heat and mass transfer phenomena, including diffusion, convection, and structural effects such as porosity and capillarity, which are not adequately captured by simplified kinetic or single-mechanism models [116]. The wide variation in A value, especially for SB, reflects the kinetic compensation effect, where increases in Ea are offset by higher frequency factors.

The devolatilization stage represents the main decomposition region and is characterised by a sharp increase in the activation energy for both biomasses, indicating that this stage is predominantly governed by the chemical breakdown of lignocellulosic components. This behaviour is consistent with established pyrolysis mechanisms, where thermal degradation proceeds through the cracking of functional groups within cellulose, hemicellulose, and lignin structures [117]. Sawdust consistently exhibits higher activation energy values (~33–84 kJ/mol) compared to sugarcane bagasse (~22–66 kJ/mol), reflecting its greater thermal resistance. This can be attributed to the higher lignin content and more ordered cellulose structure of woody biomass, as lignin decomposition occurs over a broader temperature range and requires greater energy due to its complex aromatic network [117]. This is further supported by the fact that biomass pyrolysis is governed by the combined contributions of its structural components, reinforcing the notion that devolatilization is a chemically controlled stage dominated by bond-breaking reactions [118]. In contrast, bagasse, with higher hemicellulose content and lower structural rigidity, decomposes more readily. The R^2 values in this stage are the highest (~0.94–0.98), showing that devolatilization is the most kinetically well-defined region. The reaction-order model R2 (for sugarcane bagasse) and diffusion model D6 (for sawdust) provide strong fits based on their R^2 values (0.9831 for SB and 0.9663 for SD), indicating that both chemical reaction and volatile diffusion contribute to the mechanism. The observed increase in pre-exponential factors underscores the complexity of concurrent reactions during active pyrolysis, consistent

with the multi-step nature of biomass degradation, which involves competing and parallel mechanisms [119].

In the char formation stage, the kinetic behaviour shifts significantly, with lower activation energies for diffusion and contraction models and very high R^2 values (up to ~0.99), indicating excellent model fits [120]. This confirms that the process becomes diffusion-controlled, governed by slow structural rearrangements, carbonisation, and limited reactive sites within the residual. The diffusion model D5 best describes this stage for both biomasses, whereas reaction-order models perform poorly, especially for bagasse, due to the heterogeneous, transport-limited nature of char decomposition. The relatively low A values also support the slow kinetics of this stage.

When comparing multi-stage and global single-stage approaches, the multi-stage method yields higher, more realistic activation energies (62.9 kJ/mol for sawdust and 42.3 kJ/mol for bagasse), whereas the global approach yields lower values that do not capture individual reaction stages (Table 6). This confirms that multistage kinetic modelling is more suitable for accurately describing biomass pyrolysis and aligns with literature recommendations for reactor design and process modelling [117,118].

3.6. Activation Thermodynamic Parameters

Changes in enthalpy (ΔH*), Gibbs free energy (ΔG*), and entropy (ΔS*) were calculated for both sawdust and sugarcane bagasse across specific temperature intervals, utilising data from the kinetic analysis. Due to the passive carbonisation dynamics and the absence of a distinct DTG peak within stage 3 (450–900 °C), the midpoint temperature of 675 °C was adopted as the representative reaction temperature for the calculation of thermodynamic parameters (ΔH*, ΔG*, and ΔS*) for this stage. This approach effectively represents the average thermal state of the continuous, steady-state degradation phase while preventing the mathematical skewing of Gibbs free energy calculations that would otherwise occur by utilising boundary extremes [63,104].

The results are summarised in Table 7. These metrics offer a deeper understanding of the biomass's energy demands and its thermal stability during pyrolysis [66].

Table 7. Thermodynamic data for sawdust and sugarcane bagasse.

Stage	Biomass	ΔH* (kJ/mol)	ΔG* (kJ/mol)	ΔS* (kJ/mol)
1: drying				
	Sawdust	27.3270	59.6805	−0.098
	Sugarcane bagasse	48.5701	58.7305	−0.0291
2: devolatilization				
	Sawdust	69.8734	80.0525	−0.016
	Sugarcane bagasse	40.1265	59.2099	−0.0311
3: char formation				
	Sawdust	0.6453	123.5474	−0.1293
	Sugarcane bagasse	1.5015	121.4727	−0.1266
Total (based on a multi-stage approach)				
	Sawdust	57.5667	83.9462	−0.03743
	Sugarcane bagasse	37.0327	64.9329	−0.0398
Full temperature range (25–900 °C)				
	Sawdust	17.9058	65.6215	−0.0765
	Sugarcane bagasse	24.2684	61.1072	−0.0599

In the drying stage, sugarcane bagasse shows a higher ΔH* of 48.57 kJ/mol than sawdust (27.33 kJ/mol), indicating that more energy is required to remove moisture from bagasse, likely due to stronger moisture retention within its fibrous structure. This is consistent with the reported drying behaviour of bagasse, where higher moisture content and internal mass-transfer resistance increase the energy required for moisture removal [114].

The high positive ΔG* values for both SD and SB indicate that the drying process is non-spontaneous under standard conditions without external energy input, consistent with the need for heat. Negative ΔS* values imply a decrease in entropy, indicating increased order as moisture is removed.

The devolatilization stage is the most thermodynamically demanding, with sawdust showing higher ΔH* (69.87 kJ/mol) and ΔG* (80.05 kJ/mol) than sugarcane bagasse (40.13 kJ/mol and 59.21 kJ/mol), indicating more energy-intensive devolatilization and greater thermal resistance. This indicates that sawdust possesses a more thermally stable molecular structure. This aligns with the established relationship between higher activation energy and increased energy demand during biomass conversion [23,114]. The small negative ΔS* values again indicate a slight decrease in disorder during volatile release.

In the char formation stage, ΔH* becomes very low (0.65 and 1.50 kJ/mol), ΔG* reaches its highest values (123.55 kJ/mol and 121.47 kJ/mol), and ΔS* is strongly negative (−0.1293 and −0.1266 kJ/mol·K) for sawdust and bagasse, respectively. This indicates a slightly endothermic process, but one that is strongly non-spontaneous, associated with the formation of more ordered and stable carbon structures. The negative entropy change reflects increasing structural ordering due to polycondensation and the formation of polyaromatic carbon structures during pyrolysis, as evidenced by the enhancement of aryl carbon and the development of polycyclic aromatic hydrocarbon units [117]. This also supports the multi-stage nature of biomass pyrolysis, where char formation represents a later, structurally reorganised phase [118].

The multi-stage analysis shows that the total energy required to form the activated complexes during the pyrolysis process is the sum of the energy requirements at each stage. Sawdust consumes more energy overall (higher ΔH* and ΔG*) than sugarcane bagasse, consistent with earlier findings. The positive ΔG* indicates that the overall process remains non-spontaneous and requires external energy input. However, over the entire temperature range, the overall energy and entropy changes are lower than the multi-stage total, possibly due to thermal effects at higher temperatures. These findings suggest that, compared to the single-stage method, the multi-stage method offers a deeper insight into the thermal requirement to form activated complexes during the pyrolysis of both biomass types [14,117,118].

Understanding these activation thermodynamic parameters helps optimise processing conditions. Since the process is thermodynamically endothermic and non-spontaneous, energy management strategies are essential for efficient biomass utilisation. The differences among biomass types highlight the importance of selecting feedstock based on energy requirements and process efficiency.

4. Discussion

The kinetic parameters obtained in this study for Nigerian sawdust (SD) and sugarcane bagasse (SB) show significant variations from those reported in existing literature focused on South American and Asian varieties, highlighting differences in local feedstocks. For example, the activation energy (Ea) for Nigerian SB (42.27 kJ/mol) is significantly smaller than the Ea values reported for the Brazilian (126–168 kJ/mol) [15,121] and Chinese varieties (91–104 kJ/mol) [117,121]. Similarly, the Ea for Nigerian SD (62.90 kJ/mol) shows a significant reduction compared to the literature values for Indian wood waste (148–171 kJ/mol) [96] and Moroccan wood waste (168 kJ/mol) [95]. While these variations are probably influenced by a combination of unknown crop cultivars, wood species mixtures, and environmental conditions, they underscore the necessity of characterising region-specific waste streams for localised bioenergy applications. Furthermore, the shift from the commonly assumed first-order reaction (R1) to the more complex diffusion-based (D6) and higher-order (R2) reaction

models is indicative of specific structural characteristics, such as the highly porous structure observed in the SEM micrographs, that have evolved under the Nigerian climate. These results empirically address the research gap: that the engineering of bioenergy production for Sub-Saharan countries using kinetic data from other countries may overestimate energy requirements and probably lead to poor reactor design.

5. Conclusions

This study investigated the thermal, kinetic, and thermodynamic properties of sawdust (SD) and sugarcane bagasse (SB) from Nigeria using thermogravimetric analysis (TGA) and the Coats-Redfern method to provide a detailed understanding of how these biomasses behave during pyrolysis. The study shows that although both SD and SB are highly suitable for bioenergy production, their optimal conversion pathways differ due to their distinct physicochemical properties. The comprehensive pyrolysis index establishes that both biomasses are highly reactive and viable thermochemical feedstocks, with SD possessing a marginal advantage in ease of ignition and total energy conversion. However, their internal mass-transfer and volatile release mechanisms diverge sharply during active decomposition. SD functions as a thermally stable, uniform performer; its elevated pyrolysis stability index (1002.04%/$^{\circ}C^2$) and low devolatilization index (1.2416 $\times$ 10^{-7}%/C^3) verify that its organised, parallel fibre channels degrade systematically. This behaviour minimises internal vapour pressure and prevents volatile cracking, leading to a suppressed char yield (about 17%) and an optimised pathway for primary bio-oil vapour recovery. Conversely, SB exhibits a high devolatilization index (5.062 $\times$ 10^{-7}%/C^3) and low stability index (869.27%/C^2), reflecting a sudden, chaotic structural collapse that triggers an explosive release of volatile matter. Because these rapid bursts are physically restricted by SB's dense, irregular granular matrix, the resulting intra-particle vapour retention forces secondary re-polymerisation and cracking reactions. This fundamentally drives the higher accumulation of solid residue, culminating in an elevated char yield (about 24%) at 900 °C. However, further studies involving product yield and quality analyses are recommended to validate these potential applications.

Thermodynamic analysis confirms that the formation of activated complexes by both biomasses is non-spontaneous and endothermic, highlighting the importance of efficient energy management for optimal utilisation. The diffusion models D6 and D5 best describe the drying and char-formation stages, respectively, for both biomasses, while the reaction-order model R2 and the diffusion model D6 provide robust fits for SB and SD, respectively. This underlines the multi-mechanistic nature of biomass degradation and the importance of using stage-specific kinetic models for accurate process modelling. The kinetic parameters obtained in this study for Nigerian sawdust (SD) and sugarcane bagasse (SB) show significant variations from existing literature focused on South American and Asian varieties, highlighting the need for indigenous empirical data.

This study advances the understanding of the thermal conversion of these Nigerian biomasses by demonstrating that feedstock-specific physicochemical characteristics significantly influence pyrolysis behaviour, reaction mechanisms, and energy requirements. The generated kinetic and thermodynamic parameters provide locally relevant design data for modelling and optimising pyrolysis reactors, while the multi-stage kinetic analysis highlights the importance of accounting for the heterogeneous decomposition behaviour of lignocellulosic biomass. These findings support the development of efficient biomass valorisation strategies and contribute to the broader implementation of sustainable bioenergy technologies in Nigeria and other Sub-Saharan African countries. Future studies will consider the combined effect of blending sawdust with sugarcane bagasse during their pyrolysis.

Author Contributions: Conceptualization, P.A. and R.O.; methodology, P.A. and R.O.; software, P.A.; formal analysis, P.A. and R.O.; resources, P.A. and R.O.; data curation, P.A. and R.O.; writing—original draft preparation, P.A. and R.O.; writing—review and editing, P.A. and R.O. All authors have read and agreed to the published version of the manuscript.

Funding: This research received no external funding.

Data Availability Statement: The original contributions presented in this study are included in the article. Further inquiries can be directed to the corresponding author.

Acknowledgments: The authors would like to thank the World Bank Centre of Excellence in Reproductive Health Initiative (CERHI), University of Benin and the Energy and Materials Research Laboratory, University of Johannesburg, for providing administrative support and laboratory facilities. During the preparation of this work, the authors used an artificial intelligence tool (GPT–5.6) to improve the language and readability. After using this tool, the authors reviewed and edited the content as needed and take full responsibility for the content of the publication.

Conflicts of Interest: The authors declare no conflicts of interest.

References

1. Udokpoh, U.; Nnaji, C. Reuse of Sawdust in Developing Countries in the Light of Sustainable Development Goals. *Recent Prog. Mater.* **2023**, *5*, 6. [CrossRef]
2. Shobajo, A.; Chubur, V.; Roubík, H. Potential of sugarcane bagasse as feedstock for biogas production in Nigeria. *Biofuels Bioprod. Biorefining* **2025**, *19*, 2092–2104. [CrossRef]
3. Akankali, J.A.; Davies, I.C.; Blessing, D. Assesment of Sawmill and other Associated Wastes on the Water Quality of Ilo-Abuchi Creek, Rivers State, Niger Delta. *Asian J. Fish. Aquat. Res.* **2022**, *17*, 1–13. [CrossRef]
4. Fagbenro, O.; Abdulfatai, K. Review on the Environmental Impact of Saw Mill Waste Discharges in Nigeria. *LAUTECH J. Civ. Environ. Stud.* **2018**, *1*, 75–80. [CrossRef]
5. Bakari, R.; Asha, R.; Hossein, M.; Huang, X.; Islam, N.F.; Liew, R.K.; Narayan, M.; Lam, S.S.; Sarma, H. Converting food waste to biofuel: A sustainable energy solution for Sub-Saharan Africa. *Sustain. Chem. Environ.* **2024**, *7*, 100126. [CrossRef]
6. Bongomin, O.; Nzila, C.; Mwasiagi, J.I.; Maube, O. Exploring Insights in Biomass and Waste Gasification via Ensemble Machine Learning Models and Interpretability Techniques. *Int. J. Energy Res.* **2024**, *2024*, 6087208. [CrossRef]
7. Elhenawy, Y.; Fouad, K.; Bassyouni, M.; Al-Qabandi, O.A.; Majozi, T. Yield and energy outputs analysis of sawdust biomass pyrolysis. *Energy Convers. Manag. X* **2024**, *22*, 100583. [CrossRef]
8. Okot, D.; Bilsborrow, P.; Phan, A. Thermo-chemical behaviour of maize cob and bean straw briquettes. *Energy Convers. Manag. X* **2022**, *16*, 100313. [CrossRef]
9. Kalak, T. Potential Use of Industrial Biomass Waste as a Sustainable Energy Source in the Future. *Energies* **2023**, *16*, 1783. [CrossRef]
10. Mariyam, S.; Parthasarathy, P.; Pradhan, S.; Al-Ansari, T.; McKay, G. Co-pyrolysis of biomass and binary single-use plastics: Synergy, kinetics, and thermodynamics. *Int. J. Sustain. Energy* **2024**, *43*, 2168003. [CrossRef]
11. Omol, D.; Acaye, O.; Okot, D.; Bongomin, O. Production of Fuel Oil from Municipal Plastic Wastes Using Thermal and Catalytic Pyrolysis. *J. Energy Res. Rev.* **2020**, *4*, 1–8. [CrossRef]
12. Balsora, H.K.; Kartik, S.; Rainey, T.J.; Abbas, A.; Joshi, J.B.; Sharma, A.; Chakinala, A.G. Kinetic modelling for thermal decomposition of agricultural residues at different heating rates. *Biomass Convers. Biorefinery* **2023**, *13*, 3281–3295. [CrossRef]
13. Vyas, R.; Swaminathan, P.; Chakraborty, S.; Kiran, B. Study on enhancing waste PVC management through predictive Machine Learning analysis of TGA and its economic benefits. *Energy Convers. Manag. X* **2024**, *22*, 100556. [CrossRef]
14. Fischer, O.; Lemaire, R.; Bensakhria, A. Thermogravimetric analysis and kinetic modeling of the pyrolysis of different biomass types by means of model-fitting, model-free and network modeling approaches. *J. Therm. Anal. Calorim.* **2024**, *149*, 10941–10963. [CrossRef]
15. Najafi, H.; Golrokh Sani, A.; Sobati, M.A. Thermogravimetric and thermo-kinetic analysis of sugarcane bagasse pith: A comparative evaluation with other sugarcane residues. *Sci. Rep.* **2024**, *14*, 2076. [CrossRef]
16. Steven, S.; Hernowo, P.; Nadirah, N.; Febijanto, I.; Herdioso, R.; Dharmawan, D.; Soekotjo, E.S.A.; Bindar, Y. Transformation method in determining kinetic parameters of biomass thermal decomposition from solid-state approach to volatile state approach. *Biomass Bioenergy* **2024**, *183*, 107171. [CrossRef]
17. Arumugam, D.B.; Ganesan, M.C. Catalytic co-pyrolysis of bauhinia purpurea seed and waste medical plastics for sustainable biofuel production: Kinetic analysis and prediction modeling. *Process Saf. Environ. Prot.* **2024**, *189*, 374–386. [CrossRef]

18. Wang, Y.; Yang, S.; Bao, G.; Wang, H. Investigation on prospective bioenergy from pyrolysis of macadamia nut shell waste using multicomponent Fraser-Suzuki kinetic model, kinetic triplet and thermodynamic parameters. *J. Energy Inst.* **2024**, *114*, 101611. [CrossRef]
19. Kumar Shrivastava, D.; Prasad Chakraborty, J. Estimation of kinetic and thermodynamic parameters during thermal decomposition of raw, boiled, and torrefied banana peel through arrhenius and CR methods. *Therm. Sci. Eng. Prog.* **2024**, *53*, 102696. [CrossRef]
20. Ferfari, O.; Belaadi, A.; Bourchak, M.; Ghernaout, D.; Ajaj, R.M.; Chai, B.X. Thermal decomposition of Syagrus romanzoffiana palm fibers: Thermodynamic and kinetic studies using the coats-redfern method. *Renew. Energy* **2024**, *231*, 120928. [CrossRef]
21. Li, B.; Ng, J.-H.; Woon, K.S.; Chong, W.W.F.; Ng, K.L.A.; Lee, C.T.; Chiong, M.C.; Nge, K.S.; Mong, G.R. Comparative analysis of kinetic model-fitting methods and selection priority for horse manure pyrolysis. *Sustain. Chem. Pharm.* **2024**, *39*, 101590. [CrossRef]
22. Fatmawati, A.; Nurtono, T.; Widjaja, A. Thermogravimetric kinetic-based computation of raw and pretreated coconut husk powder lignocellulosic composition. *Bioresour. Technol. Rep.* **2023**, *22*, 101500. [CrossRef]
23. Kumar, P.; Chaunsali, P.; Vinu, R. Pyrolysis of rice husk, bagasse and wood chips blends: Distributed activation energy modelling and pyrolysate composition analysis. *Fuel* **2026**, *404*, 136116. [CrossRef]
24. Yousef, S.; Eimontas, J.; Striūgas, N.; Subadra, S.P.; Abdelnaby, M.A. Thermal degradation and pyrolysis kinetic behaviour of glass fibre-reinforced thermoplastic resin by TG-FTIR, Py-GC/MS, linear and nonlinear isoconversional models. *J. Mater. Res. Technol.* **2021**, *15*, 5360–5374. [CrossRef]
25. Ibitoye, S.E.; Mahamood, R.M.; Jen, T.-C.; Loha, C.; Akinlabi, E.T. An overview of biomass solid fuels: Biomass sources, processing methods, and morphological and microstructural properties. *J. Bioresour. Bioprod.* **2023**, *8*, 333–360. [CrossRef]
26. Parthasarathy, P.; Al-Ansari, T.; Mackey, H.R.; McKay, G. Effect of heating rate on the pyrolysis of camel manure. *Biomass Convers. Biorefinery* **2023**, *13*, 6023–6035. [CrossRef]
27. Choudhary, J.; Kumar, A.; Alawa, B.; Chakma, S. Optimization and prediction of thermodynamic parameters in co-pyrolysis of banana peel and waste plastics using AIC model and ANN modeling. *Energy Nexus* **2024**, *14*, 100302. [CrossRef]
28. Li, B.Y.; Tee, M.Y.; Nge, K.S.; Ng, A.K.L.; Chong, W.W.F.; Ng, J.-H.; Mong, G.R. Comparison kinetic analysis between coats-redfern and criado's master plot on pyrolysis of horse manure. *Chem. Eng. Trans.* **2023**, *106*, 1273–1278.
29. Tariq, R.; Saeed, S.; Riaz, M.; Saeed, S. Kinetic and thermodynamic evaluation of almond shells pyrolytic behavior using Coats–Redfern and pyrolysis product distribution model. *Energy Sources Part A Recovery Util. Environ. Eff.* **2023**, *45*, 4446–4462. [CrossRef]
30. Coats, A.W.; Redfern, J.P. Kinetic Parameters from Thermogravimetric Data. *Nature* **1964**, *201*, 68–69. [CrossRef]
31. Ebrahimi-Kahrizsangi, R.; Abbasi, M.H. Evaluation of reliability of Coats-Redfern method for kinetic analysis of non-isothermal TGA. *Trans. Nonferrous Met. Soc. China* **2008**, *18*, 217–221. [CrossRef]
32. Sivaraman, S.; Shanmugam, S.; Veerapandian, B.; Ponnusami, V. Understanding the pyrolysis kinetics, thermodynamic and environmental sustainability parameters of Sesamum indicum crop residue. *Environ. Res. Commun.* **2023**, *5*, 125013. [CrossRef]
33. Wang, K.; Shan, T.; Li, B.; Zheng, Y.; Xu, H.; Wang, C.; Tian, X. Study on pyrolysis characteristics, kinetics and thermodynamics of waste tires catalytic pyrolysis with low-cost catalysts. *Fuel* **2024**, *356*, 129644. [CrossRef]
34. Wang, S.; Wu, K.; Yu, J.; Luo, B.; Chu, C.; Zhang, H. Kinetic and thermodynamic analysis of biomass catalytic pyrolysis with nascent biochar in a two-stage reactor. *Combust. Flame* **2023**, *251*, 112671. [CrossRef]
35. Huang, J.; Wang, X.; Sun, Z.e.; Song, L.; Wang, J. Interpretable machine learning model for activation energy prediction based on biomass properties. *Therm. Sci. Eng. Prog.* **2024**, *53*, 102734. [CrossRef]
36. Zhang, Z.; Li, Y.; Luo, L.; Yellezuome, D.; Rahman, M.M.; Zou, J.; Hu, H.; Cai, J. Insight into kinetic and Thermodynamic Analysis methods for lignocellulosic biomass pyrolysis. *Renew. Energy* **2023**, *202*, 154–171. [CrossRef]
37. Chinenye Divine, D.; Hubert, S.; Epelle, E.I.; Ojo, A.U.; Adeleke, A.A.; Ogbaga, C.C.; Akande, O.; Okoye, P.U.; Giwa, A.; Okolie, J.A. Enhancing biomass Pyrolysis: Predictive insights from process simulation integrated with interpretable Machine learning models. *Fuel* **2024**, *366*, 131346. [CrossRef]
38. Gupta, R.; Ouderji, Z.H.; Uzma; Yu, Z.; Sloan, W.T.; You, S. Machine learning for sustainable organic waste treatment: A critical review. *npj Mater. Sustain.* **2024**, *2*, 5. [CrossRef]
39. Zhang, P.; Zhang, T.; Zhang, J.; Liu, H.; Chicaiza-Ortiz, C.; Lee, J.T.E.; He, Y.; Dai, Y.; Tong, Y.W. A machine learning assisted prediction of potential biochar and its applications in anaerobic digestion for valuable chemicals and energy recovery from organic waste. *Carbon Neutrality* **2024**, *3*, 2. [CrossRef]
40. Liu, J.; Lyu, H.; Cheng, C.; Xu, Z.; Zhang, W. Enhancing pyrolysis process monitoring and prediction for biomass: A machine learning approach. *Fuel* **2024**, *362*, 130873. [CrossRef]
41. Osman, A.I.; Nasr, M.; Farghali, M.; Rashwan, A.K.; Abdelkader, A.; Al-Muhtaseb, A.a.H.; Ihara, I.; Rooney, D.W. Optimizing biodiesel production from waste with computational chemistry, machine learning and policy insights: A review. *Environ. Chem. Lett.* **2024**, *22*, 1005–1071. [CrossRef]

42. Sánchez-Ávila, N.; Cardarelli, A.; Carmona-Cabello, M.; Dorado, M.P.; Pinzi, S.; Barbanera, M. Kinetic and thermodynamic behavior of co-pyrolysis of olive pomace and thermoplastic waste via thermogravimetric analysis. *Renew. Energy* **2024**, *230*, 120880. [CrossRef]
43. Amoloye, M.; Abdulkareem, S.; Adeniyi, A. Thermo-kinetics, thermodynamics, and ANN modeling of the pyrolytic behaviours of Corn Cob, Husk, Leaf, and Stalk using thermogravimetric analysis. *Chem. Prod. Process Model.* **2023**, *18*, 859–876. [CrossRef]
44. Chen, R.; Yu, X.; Dong, B.; Dai, X. Sludge-to-energy approaches based on pathways that couple pyrolysis with anaerobic digestion (thermal hydrolysis pre/post-treatment): Energy efficiency assessment and pyrolysis kinetics analysis. *Energy* **2020**, *190*, 116240. [CrossRef]
45. Osman, A.I.; Fang, B.; Zhang, Y.; Liu, Y.; Yu, J.; Farghali, M.; Rashwan, A.K.; Chen, Z.; Chen, L.; Ihara, I.; et al. Life cycle assessment and techno-economic analysis of sustainable bioenergy production: A review. *Environ. Chem. Lett.* **2024**, *22*, 1115–1154. [CrossRef]
46. Vanisree, G.S.; Chandran, A.M.; Aparna, K. Investigation on thermochemical characteristics and pyrolysis kinetics of lignocellulosic biomass for biofuel production feasibility. *Biomass Convers. Biorefinery* **2025**, *15*, 28667–28685. [CrossRef]
47. Kumar, V.K.; Hallad, S.C.; Panwar, N.L. Thermogravimetric pyrolysis investigation of pistachio shell for its potential of thermal properties, kinetics and thermodynamics. *Discov. Energy* **2024**, *4*, 7. [CrossRef]
48. Rashd, J.A.; Lalung, J.; Kassim, M.A.; Wijaya, D.; Allzrag, A.M.M.; Shaah, M.A. Kinetics and thermodynamic studies on biodiesel synthesis via Soxhlet extraction of Scenedesmus parvus algae oil. *Energy Convers. Manag. X* **2024**, *23*, 100633. [CrossRef]
49. Dai, M.; Guo, T.; Hu, X.; Ma, J.; Guo, Q. Simulation of a 1MWth biomass chemical looping gasification process based on kinetic and pyrolysis models. *Int. J. Hydrogen Energy* **2024**, *80*, 298–307. [CrossRef]
50. Lingamdinne, L.P.; Angaru, G.K.R.; Pal, C.A.; Koduru, J.R.; Karri, R.R.; Mubarak, N.M.; Chang, Y.-Y. Insights into kinetics, thermodynamics, and mechanisms of chemically activated sunflower stem biochar for removal of phenol and bisphenol-A from wastewater. *Sci. Rep.* **2024**, *14*, 4267. [CrossRef]
51. Nath, S. Biotechnology and biofuels: Paving the way towards a sustainable and equitable energy for the future. *Discov. Energy* **2024**, *4*, 8. [CrossRef]
52. Samuel Olugbenga, O.; Goodness Adeleye, P.; Blessing Oladipupo, S.; Timothy Adeleye, A.; Igenepo John, K. Biomass-derived biochar in wastewater treatment—A circular economy approach. *Waste Manag. Bull.* **2024**, *1*, 1–14. [CrossRef]
53. Temireyeva, A.; Sarbassov, Y.; Shah, D. Process simulation of flax straw pyrolysis with kinetic reaction Model: Experimental validation and exergy analysis. *Fuel* **2024**, *367*, 131494. [CrossRef]
54. Adeleke, A.A.; Petrus, N.; Ayuba, S.; Yahya, A.M.; Ikubanni, P.P.; Okafor, I.S.; Emmanuel, S.S.; Olosho, A.I.; Adesibikan, A.A. Nigerian Biomass for Bioenergy Applications: A Review on the Potential and Challenges. *J. Renew. Mater.* **2023**, *11*, 4123–4141. [CrossRef]
55. Akinrinola, F.S.; Darvell, L.I.; Jones, J.M.; Williams, A.; Fuwape, J.A. Characterization of Selected Nigerian Biomass for Combustion and Pyrolysis Applications. *Energy Fuels* **2014**, *28*, 3821–3832. [CrossRef]
56. Olivia, E.-I.N.; Oti Wilberforce, J. Characterization of Selected Nigerian Indigenous Biomass Wastes for Their Suitability in Biofuel Production. *Int. J. Pharm. Sci. Invent.* **2017**, *6*, 1–8.
57. Balogun, K.; Lasode, M.; Onokwai, A.; Ezugwu, C.; Olayanju, T.; Osueke, C. Elemental analysis and combustion characteristics evaluation of Nigerian biomass resources. *Int. J. Mech. Eng. Technol. (IJMET)* **2019**, *10*, 1522–1527.
58. Efetobor, U.J.; Ikpeseni, S.C.; Sada, S.O. Determination of Proximate, Ultimate and Structural Properties of Elephant Grass as Biomass Material for Bio-oil Production. *J. Appl. Sci. Environ. Manag.* **2022**, *26*, 1903–1907. [CrossRef]
59. de Palma, K.R.; García-Hernando, N.; Silva, M.A.; Tomaz, E.; Soria-Verdugo, A. Pyrolysis and Combustion Kinetic Study and Complementary Study of Ash Fusibility Behavior of Sugarcane Bagasse, Sugarcane Straw, and Their Pellets—Case Study of Agro-Industrial Residues. *Energy Fuels* **2019**, *33*, 3227–3238. [CrossRef]
60. Dias, S.d.A.; Toscano Miranda, N.; Maciel Filho, R.; Sphaier, L.A.; Castillo Santiago, Y. Sugarcane Bagasse Fast Pyrolysis: Pilot Plant Challenges. *Processes* **2025**, *13*, 2116. [CrossRef]
61. Zhang, S.; Gao, Y.; Tong, H.; Dong, Y.; Qi, G.; Wang, P. The Pyrolysis Characteristics of Bagasse Were Studied by TG-MS-FTIR. *Processes* **2024**, *12*, 2494. [CrossRef]
62. Lei, J.; Liu, X.; Xu, B.; Liu, Z.; Fu, Y. Combustion Characteristics, Kinetics and Thermodynamics of Peanut Shell for Its Bioenergy Valorization. *Processes* **2024**, *12*, 1022. [CrossRef]
63. Lei, J.; Wang, Y.; Wang, Q.; Deng, S.; Fu, Y. Evaluation of Kinetic and Thermodynamic Parameters of Pyrolysis and Combustion Processes for Bamboo Using Thermogravimetric Analysis. *Processes* **2024**, *12*, 2458. [CrossRef]
64. El-Sayed, S.A.; Khass, T.M.; Mostafa, M.E. Thermal degradation behaviour and chemical kinetic characteristics of biomass pyrolysis using TG/DTG/DTA techniques. *Biomass Convers. Biorefinery* **2024**, *14*, 17779–17803. [CrossRef]
65. Escalante, J.; Chen, W.-H.; Tabatabaei, M.; Hoang, A.T.; Kwon, E.E.; Andrew Lin, K.-Y.; Saravanakumar, A. Pyrolysis of lignocellulosic, algal, plastic, and other biomass wastes for biofuel production and circular bioeconomy: A review of thermogravimetric analysis (TGA) approach. *Renew. Sustain. Energy Rev.* **2022**, *169*, 112914. [CrossRef]

66. Gajera, B.; Tyagi, U.; Sarma, A.K.; Jha, M.K. Impact of torrefaction on thermal behavior of wheat straw and groundnut stalk biomass: Kinetic and thermodynamic study. *Fuel Commun.* **2022**, *12*, 100073. [CrossRef]
67. Gupta, G.K.; Gupta, P.K.; Mondal, M.K. Experimental process parameters optimization and in-depth product characterizations for teak sawdust pyrolysis. *Waste Manag.* **2019**, *87*, 499–511. [CrossRef]
68. Zhang, J.; Liu, J.; Evrendilek, F.; Zhang, X.; Buyukada, M. TG-FTIR and Py-GC/MS analyses of pyrolysis behaviors and products of cattle manure in CO_2 and N_2 atmospheres: Kinetic, thermodynamic, and machine-learning models. *Energy Convers. Manag.* **2019**, *195*, 346–359. [CrossRef]
69. Huang, H.; Liu, J.; Liu, H.; Evrendilek, F.; Buyukada, M. Pyrolysis of water hyacinth biomass parts: Bioenergy, gas emissions, and by-products using TG-FTIR and Py-GC/MS analyses. *Energy Convers. Manag.* **2020**, *207*, 112552. [CrossRef]
70. Ahmed, S.F.; Rafa, S.J.; Mehjabin, A.; Tasannum, N.; Ahmed, S.; Mofijur, M.; Lichtfouse, E.; Almomani, F.; Badruddin, I.A.; Kamangar, S. Bio-oil from microalgae: Materials, production, technique, and future. *Energy Rep.* **2023**, *10*, 3297–3314. [CrossRef]
71. Igliński, B.; Kujawski, W.; Kiełkowska, U. Pyrolysis of Waste Biomass: Technical and Process Achievements, and Future Development—A Review. *Energies* **2023**, *16*, 1829. [CrossRef]
72. Yi, Q.; Qi, F.; Cheng, G.; Zhang, Y.; Xiao, B.; Hu, Z.; Liu, S.; Cai, H.; Xu, S. Thermogravimetric analysis of co-combustion of biomass and biochar. *J. Therm. Anal. Calorim.* **2013**, *112*, 1475–1479. [CrossRef]
73. Bongomin, O.; Nzila, C.; Igadwa Mwasiagi, J.; Maube, O. Comprehensive thermal properties, kinetic, and thermodynamic analyses of biomass wastes pyrolysis via TGA and Coats-Redfern methodologies. *Energy Convers. Manag. X* **2024**, *24*, 100723. [CrossRef]
74. Uddin Monir, M.; Muntasir Shovon, S.; Ahamed Akash, F.; Habib, M.A.; Techato, K.; Abd Aziz, A.; Chowdhury, S.; Eka Prasetya, T.A. Comprehensive characterization and kinetic analysis of coconut shell thermal degradation: Energy potential evaluated via the Coats-Redfern method. *Case Stud. Therm. Eng.* **2024**, *55*, 104186. [CrossRef]
75. Wu, S.; Wang, Q.; Cui, D.; Sun, H.; Yin, H.; Xu, F.; Wang, Z. Evaluation of fuel properties and combustion behaviour of hydrochar derived from hydrothermal carbonisation of agricultural wastes. *J. Energy Inst.* **2023**, *108*, 101209. [CrossRef]
76. Gajera, Z.R.; Verma, K.; Tekade, S.P.; Sawarkar, A.N. Kinetics of co-gasification of rice husk biomass and high sulphur petroleum coke with oxygen as gasifying medium via TGA. *Bioresour. Technol. Rep.* **2020**, *11*, 100479. [CrossRef]
77. Liang, W.; Wang, G.; Jiao, K.; Ning, X.; Zhang, J.; Guo, X.; Li, J.; Wang, C. Conversion mechanism and gasification kinetics of biomass char during hydrothermal carbonization. *Renew. Energy* **2021**, *173*, 318–328. [CrossRef]
78. Balasundram, V.; Ibrahim, N.; Kasmani, R.M.; Hamid, M.K.A.; Isha, R.; Hasbullah, H.; Ali, R.R. Thermogravimetric catalytic pyrolysis and kinetic studies of coconut copra and rice husk for possible maximum production of pyrolysis oil. *J. Clean. Prod.* **2017**, *167*, 218–228. [CrossRef]
79. Khawam, A.; Flanagan, D.R. Solid-State Kinetic Models: Basics and Mathematical Fundamentals. *J. Phys. Chem. B* **2006**, *110*, 17315–17328. [CrossRef]
80. Ali, I.; Tariq, R.; Naqvi, S.R.; Khoja, A.H.; Mehran, M.T.; Naqvi, M.; Gao, N. Kinetic and thermodynamic analyses of dried oily sludge pyrolysis. *J. Energy Inst.* **2021**, *95*, 30–40. [CrossRef]
81. Balogun, A.O.; Adeleke, A.A.; Ikubanni, P.P.; Adegoke, S.O.; Alayat, A.M.; McDonald, A.G. Kinetics modeling, thermodynamics and thermal performance assessments of pyrolytic decomposition of Moringa oleifera husk and Delonix regia pod. *Sci. Rep.* **2021**, *11*, 13862. [CrossRef]
82. Hai, A.; Bharath, G.; Daud, M.; Rambabu, K.; Ali, I.; Hasan, S.W.; Show, P.; Banat, F. Valorization of groundnut shell via pyrolysis: Product distribution, thermodynamic analysis, kinetic estimation, and artificial neural network modeling. *Chemosphere* **2021**, *283*, 131162. [CrossRef]
83. Vyazovkin, S.; Burnham, A.K.; Favergeon, L.; Koga, N.; Moukhina, E.; Pérez-Maqueda, L.A.; Sbirrazzuoli, N. ICTAC Kinetics Committee recommendations for analysis of multi-step kinetics. *Thermochim. Acta* **2020**, *689*, 178597. [CrossRef]
84. Álvarez, A.; Pizarro, C.; García, R.; Bueno, J.L.; Lavín, A.G. Determination of kinetic parameters for biomass combustion. *Bioresour. Technol.* **2016**, *216*, 36–43. [CrossRef]
85. Zsinka, V.; Tarcsay, B.L.; Miskolczi, N. Determination of Kinetic and Thermodynamic Parameters of Biomass Gasification with TG-FTIR and Regression Model Fitting. *Energies* **2024**, *17*, 1875. [CrossRef]
86. Mishra, R.K.; Vinu, R. Pyrolysis characteristics and kinetic investigation of waste groundnut shells using thermogravimetric analyzer, Py-FTIR, and Py-GC-MS. *J. Anal. Appl. Pyrolysis* **2024**, *179*, 106514. [CrossRef]
87. Adeoye, A.O.; Quadri, R.O.; Lawal, O.S. Wet synthesis, characterization of goethite nanoparticles and its application in catalytic pyrolysis of palm kernel shell in TGA. *Results Surf. Interfaces* **2023**, *11*, 100118. [CrossRef]
88. Alashmawy, M.M.; Hassan, H.S.; Ookawara, S.A.; Elwardany, A.E. Thermal decomposition characteristics and study of the reaction kinetics of tea-waste. *Biomass Convers. Biorefinery* **2023**, *13*, 9487–9505. [CrossRef]
89. Shahdan, N.A.; Balasundram, V.; Ibrahim, N.; Isha, R.; Manan, Z.A. Catalytic Co-pyrolysis of empty fruit bunch and high-density polyethylene mixtures over rice husk ash: Thermogravimetric, kinetic and thermodynamic analyses. *Clean. Eng. Technol.* **2022**, *9*, 100538. [CrossRef]

90. Bahú, J.O.; de Oliveira, R.A.; De Souza, L.M.A.; Rivera, E.C.; Felisbino, R.F.; Maciel Filho, R.; Tovar, L.P. Kinetic study of thermal decomposition of sugarcane bagasse pseudo-components at typical pretreatment conditions: Simulations of opportunities towards the establishment of a feasible primary biorefining. *Clean. Chem. Eng.* **2022**, *4*, 100074. [CrossRef]
91. Zanatta, E.R.; Reinehr, T.O.; Awadallak, J.A.; Kleinübing, S.J.; dos Santos, J.B.O.; Bariccatti, R.A.; Arroyo, P.A.; da Silva, E.A. Kinetic studies of thermal decomposition of sugarcane bagasse and cassava bagasse. *J. Therm. Anal. Calorim.* **2016**, *125*, 437–445. [CrossRef]
92. El-Naggar, M.A.; Mousa, M.A.; Reda, S.M.; Emara, M.M. Thermal decomposition behavior and kinetics for pyrolysis and catalytic pyrolysis of sugarcane bagasse. *Sustain. Chem. Pharm.* **2025**, *44*, 101976. [CrossRef]
93. Khan, M.N.; Ahmad, A.; Rehman, N.; Kelestemur, S.; Tariq, M.; Jan, A.K.; Ahmad, S.; Eisele, D.M.; Syed, W.; Al-Rawi, M.B.A. Extraction and characterization of cellulose and cellulose nanocrystals from the stalks of Marrubium vulgare plant. *Carbohydr. Polym. Technol. Appl.* **2025**, *11*, 100947. [CrossRef]
94. Guida, M.; Lanaya, S.; Rbihi, Z.; Hannioui, A. Thermal degradation behaviors of sawdust wood waste: Pyrolysis kinetic and mechanism. *J. Mater. Environ. Sci.* **2019**, *10*, 742–755.
95. Mishra, R.K.; Mohanty, K. Pyrolysis kinetics and thermal behavior of waste sawdust biomass using thermogravimetric analysis. *Bioresour. Technol.* **2018**, *251*, 63–74. [CrossRef]
96. Weihong, Z.; Bin, B.; Guanyi, C.; Longlong, M.; Beibei, Y. Thermogravimetric characteristics and kinetics of sawdust pyrolysis catalyzed by potassium salt during the process of hydrogen preparation. *Int. J. Hydrogen Energy* **2019**, *44*, 15863–15870. [CrossRef]
97. Apaydın Varol, E.; Mutlu, Ü. TGA-FTIR Analysis of Biomass Samples Based on the Thermal Decomposition Behavior of Hemicellulose, Cellulose, and Lignin. *Energies* **2023**, *16*, 3674. [CrossRef]
98. Asadieraghi, M.; Wan Daud, W.M.A. Characterization of lignocellulosic biomass thermal degradation and physiochemical structure: Effects of demineralization by diverse acid solutions. *Energy Convers. Manag.* **2014**, *82*, 71–82. [CrossRef]
99. Ornaghi, H.L.; Ornaghi, F.G.; Neves, R.M.; Monticeli, F.; Bianchi, O. Mechanisms involved in thermal degradation of lignocellulosic fibers: A survey based on chemical composition. *Cellulose* **2020**, *27*, 4949–4961. [CrossRef]
100. Kostryukov, S.G.; Matyakubov, H.B.; Masterova, Y.Y.; Kozlov, A.S.; Pryanichnikova, M.K.; Pynenkov, A.A.; Khluchina, N.A. Determination of Lignin, Cellulose, and Hemicellulose in Plant Materials by FTIR Spectroscopy. *J. Anal. Chem.* **2023**, *78*, 718–727. [CrossRef]
101. Faix, O. Fourier Transform Infrared Spectroscopy. In *Methods in Lignin Chemistry*; Lin, S.Y., Dence, C.W., Eds.; Springer: Berlin/Heidelberg, Germany, 1992; pp. 233–241.
102. Dong, Q.; Zhang, Y.; Li, M.; Li, B.; Li, C.; Liu, D. CO_2 capture and microwave absorption by pine sawdust biochars obtained via molten salt pyrolysis. *Biomass Bioenergy* **2025**, *201*, 108053. [CrossRef]
103. Liu, B.-S.; Yao, C.-J.; Qi, J.-L.; Liu, Y.-Q.; Xu, L.; Hou, J.-X. Experimental investigation on pyrolysis products and pore structure characteristics of organic-rich shale heated by supercritical carbon dioxide. *Pet. Sci.* **2024**, *21*, 2393–2406. [CrossRef]
104. Gaber H. Saif, A.; Wahid, S.; Ali, M. Pyrolysis of Sugarcane Bagasse: The Effects of Process Parameters on the Product Yields. *Mater. Sci. Forum* **2020**, *1008*, 159–167. [CrossRef]
105. Dorez, G.; Ferry, L.; Sonnier, R.; Taguet, A.; Lopez-Cuesta, J.M. Effect of cellulose, hemicellulose and lignin contents on pyrolysis and combustion of natural fibers. *J. Anal. Appl. Pyrolysis* **2014**, *107*, 323–331. [CrossRef]
106. Zhang, S.; Chen, Z.-d.; Chen, X.-j.; Gong, X.-z. Effects of ash/K_2CO_3/Fe_2O_3 on ignition temperature and combustion rate of demineralized anthracite. *J. Fuel Chem. Technol.* **2014**, *42*, 166–174. [CrossRef]
107. Zhu, L.; Zhong, Z. Effects of cellulose, hemicellulose and lignin on biomass pyrolysis kinetics. *Korean J. Chem. Eng.* **2020**, *37*, 1660–1668. [CrossRef]
108. Mahmud, M.A.; Anannya, F.R. Sugarcane bagasse—A source of cellulosic fiber for diverse applications. *Heliyon* **2021**, *7*, e07771. [CrossRef]
109. Alcazar-Ruiz, A.; Ortiz, M.L.; Sanchez-Silva, L.; Dorado, F. Catalytic effect of alkali and alkaline earth metals on fast pyrolysis pre-treatment of agricultural waste. *Biofuels Bioprod. Biorefining* **2021**, *15*, 1473–1484. [CrossRef]
110. Safar, M.; Lin, B.-J.; Chen, W.-H.; Langauer, D.; Chang, J.-S.; Raclavska, H.; Pétrissans, A.; Rousset, P.; Pétrissans, M. Catalytic effects of potassium on biomass pyrolysis, combustion and torrefaction. *Appl. Energy* **2019**, *235*, 346–355. [CrossRef]
111. Shagali, A.A.; Mostafa, M.E.; Li, H.; Hu, S.; Xu, J.; Jiang, L.; Wang, Y.; Su, S.; Xiang, J. Pyrolysis characteristics and kinetic parameters assessment of typical agricultural residues using high heating photothermal TGA. *J. Anal. Appl. Pyrolysis* **2023**, *174*, 106109. [CrossRef]
112. Akhator, P.; Oboirien, B.; N. Borhani, T. Interaction effects between sugarcane bagasse and sawdust during their co-hydrothermal carbonisation and co-gasification. *Energy Convers. Manag. X* **2025**, *28*, 101247. [CrossRef]
113. Dendukuri, R.; Narayanan, A.; Manickam, P.; Raghuram, V. Experimental studies on the effect of moisture content and temperature on moisture effective diffusivity and activation energy of bagasse. *Energy Sources Part A Recovery Util. Environ. Eff.* **2024**, *46*, 8320–8332. [CrossRef]

114. de Cassia Santos, Y.; Martins Freitas, M.D.; Freire, F.B.; Freire, J.T.; Bitti Perazzini, M.T.; Perazzini, H. Heat and mass transfer in fluidized bed drying of acai agricultural biomass waste. *Fuel* **2025**, *399*, 135547. [CrossRef]
115. Gandía Ventura, I.; Velázquez Martí, B.; López Cortes, I.; Guerrero-Luzuriaga, S. Kinetic Models of Wood Biomass Drying in Hot Airflow Systems. *Appl. Sci.* **2024**, *14*, 6716. [CrossRef]
116. Chen, D.; Cen, K.; Zhuang, X.; Gan, Z.; Zhou, J.; Zhang, Y.; Zhang, H. Insight into biomass pyrolysis mechanism based on cellulose, hemicellulose, and lignin: Evolution of volatiles and kinetics, elucidation of reaction pathways, and characterization of gas, biochar and bio-oil. *Combust. Flame* **2022**, *242*, 112142. [CrossRef]
117. Anca-Couce, A. Reaction mechanisms and multi-scale modelling of lignocellulosic biomass pyrolysis. *Prog. Energy Combust. Sci.* **2016**, *53*, 41–79. [CrossRef]
118. Sbirrazzuoli, N. Kinetic analysis of complex chemical reactions by coupling model-free and model-fitting analysis. *Thermochim. Acta* **2023**, *719*, 179416. [CrossRef]
119. Sobek, S.; Werle, S. Kinetic modelling of waste wood devolatilization during pyrolysis based on thermogravimetric data and solar pyrolysis reactor performance. *Fuel* **2020**, *261*, 116459. [CrossRef]
120. Liborio, D.O.; Gonzalez, J.F.; Arias, S.; Mumbach, G.D.; Alves, J.L.F.; da Silva, J.C.G.; Silva, J.M.F.; Barbosa, C.M.B.M.; Carvalho, F.R.; Soares, R.R.; et al. Pyrolysis of Energy Cane Bagasse: Investigating Kinetics, Thermodynamics, and Effect of Temperature on Volatile Products. *Energies* **2023**, *16*, 5669. [CrossRef]
121. Varma, A.K.; Mondal, P. Physicochemical Characterization and Pyrolysis Kinetic Study of Sugarcane Bagasse Using Thermogravimetric Analysis. *J. Energy Resour. Technol.* **2016**, *138*, 052205. [CrossRef]

Disclaimer/Publisher's Note: The statements, opinions and data contained in all publications are solely those of the individual author(s) and contributor(s) and not of MDPI and/or the editor(s). MDPI and/or the editor(s) disclaim responsibility for any injury to people or property resulting from any ideas, methods, instructions or products referred to in the content.